

The impact of lateral boundary forcing in the CORDEX-Africa ensemble over southern Africa

Maria Chara Karypidou¹, Stefan Pieter Sobolowski², Lorenzo Sangelantoni^{3,4}, Grigory Nikulin⁵, Eleni Katragkou¹

¹ Department of Meteorology and Climatology, School of Geology, Faculty of Sciences, Aristotle University of Thessaloniki, Thessaloniki, Greece

² NORCE Norwegian Research Centre, Bjerknes Centre for Climate Research, Bergen, Norway

³ Climate Simulation and Prediction Division, Centro Euro-Mediterraneo sui Cambiamenti Climatici, Bologna 40127, Italy

⁴ Center of Excellence in Telesensing of Environment and Model Prediction of Severe Events (CETEMPS), University of L'Aquila, L'Aquila, Italy

⁵ Rossby Centre, Swedish Meteorological and Hydrological Institute, Norrköping, Sweden

Corresponding author: Maria Chara Karypidou, karypidou@geo.auth.gr

Abstract

The region of southern Africa (SAF) is among the most exposed climate change hotspots and is projected to experience severe impacts across multiple economical and societal sectors. For this reason, producing reliable projections of the expected impacts of climate change is key for local communities. In this work we use an ensemble of 19 regional climate model (RCM) simulations performed in the context of the Coordinated Regional Climate Downscaling Experiment (CORDEX) – Africa and a set of 10 global climate models (GCMs) participating in the Coupled Model Intercomparison Project Phase 5 (CMIP5), that were used as the driving GCMs in the RCM simulations. We are concerned about the degree to which RCM simulations are influenced by their driving GCMs, with regards to monthly precipitation climatologies, precipitation biases and precipitation change signal, according to the Representative Concentration Pathway (RCP) 8.5 for the end of the 21st century. We investigate the degree to which RCMs and GCMs are able to reproduce specific climatic features over SAF and over three sub-regions, namely the greater Angola region, the greater Mozambique region and the greater South Africa region. We identify that during the beginning of the rainy season, when regional processes are largely dependent on the coupling between the surface and the atmosphere, the impact of the driving GCMs on the RCMs is smaller, compared to the core of the rainy season, when precipitation is mainly controlled by the large-scale circulation. In addition, we show that RCMs are able to counteract the bias received by their driving GCMs, hence, we claim that the cascade of uncertainty over SAF is not additive, but indeed the RCMs do provide improved precipitation climatologies. The fact that certain bias patterns during the historical period (1985-2005) identified in GCMs are resolved in RCMs, provides evidence that RCMs are reliable tools for climate change impact studies over SAF.

1 Introduction

38 The region of southern Africa (SAF) is among the most exposed climate change hotspots (Diffenbaugh and Giorgi,
39 2012) and is projected to experience severe impacts across multiple economical and societal sectors (Conway et al.,
40 2015; Masipa, 2017; Shew et al., 2020). Poverty, food insecurity, and high levels of malnutrition (Misselhorn and
41 Hendriks, 2017) render SAF particularly vulnerable to the impacts of climate change (Casale et al., 2010; Luan et al.,
42 2013; Wolski et al., 2020). In addition, the population's reliance on rain-fed agriculture makes strategic planning
43 necessary, as it aims to mitigate the impact of climate change on local communities.

44 Global climate models (GCM) participating in the Coupled Model Intercomparison Project Phase 5 (CMIP5) (Taylor
45 et al., 2012) project a significant decline in annual precipitation over SAF (IPCC and Stocker, 2013), with the most
46 pronounced changes projected under representative concentration pathway 8.5 (RCP8.5) (Sillmann et al., 2013). This
47 reduction is also identified in the regional climate model (RCM) simulations performed in the context of the
48 Coordinated Regional Climate Downscaling Experiment (CORDEX) – Africa domain (Nikulin et al., 2012; Giorgi
49 and Gutowski, 2015). More specifically, according to CORDEX-Africa simulations, annual precipitation is expected
50 to decline by up to 50% by the end of the 21st century (Pinto et al., 2018), while duration of dry spells is projected to
51 increase (Dosio et al., 2019). Despite this, extreme rain events are expected to increase in frequency and intensity
52 (Pinto et al., 2016; Abiodun et al., 2019). Nevertheless, for a global warming level of 2 °C, certain parts of SAF
53 (northern Angola, Zambia, northern Mozambique, and eastern South Africa) are projected to experience precipitation
54 increase during specific times of the year (Maúre et al., 2018).

55 The question of whether or not RCMs produce demonstrable added value relative to their driving GCMs, has often
56 fueled debate between the RCM and GCM modelling communities (Lloyd et al., 2020). The outcome of the debate is
57 not binary. The literature provides ample evidence that there is indeed evidence of added value in RCMs, but it is
58 dependent on the region examined, on the season, and the climate mechanisms that are at play (Luca et al., 2016, Feser
59 et al., 2011). RCM ensembles such as those developed within CORDEX-Africa endeavor to provide added value, by
60 dynamically downscaling historical and scenario simulations originating from coarse resolution GCMs (Dosio et al.,
61 2019). The added value in RCM simulations arises as a result of their higher horizontal resolution (<50 km), which
62 makes it possible for atmospheric waves and synoptic scale disturbances to be represented in a more realistic manner.
63 An additional aspect that further contributes towards this end, is the more accurate representation of land surface
64 characteristics (topography, land use etc.) in RCMs (Di Luca et al., 2013). Moreover, the physics of an RCM can be
65 targeted for processes specific to the region it is being run for, giving it a local advantage over GCMs that may have
66 had their physics developed for global applications. Nevertheless, RCMs also are accompanied by a set of model
67 deficiencies that affect the final output of the downscaled data (Boberg and Christensen, 2012). In Sørland et al. (2018)
68 it is reported that although RCM biases are affected by the driving GCMs, they are nonetheless not additive, a result
69 that counters the common “cascade of uncertainty” criticism. Still, uncertainty arising from both the driving GCM
70 (Moalafhi et al., 2017) and the downscaling RCM affect the final product (Nikulin et al., 2012), and it is important to
71 diagnose the sources and causes of these errors (Déqué et al., 2012).

72 Attributing total uncertainty to its respective components is key for a better assessment of the reliability of RCM
73 simulations (Christensen and Kjellström, 2020). GCMs provide the lateral boundary conditions to the RCMs and each
74 RCM receives, absorbs, and modulates the received atmospheric forcing in different ways, depending on the numerical

75 formulations and parameterization schemes employed. Discerning between the signal received from the GCM and the
76 signal produced by the RCM is critical for assessing the robustness with which different modelling systems are able
77 to accurately reproduce observed climatologies and generate reliable estimates of the expected climate change. In
78 addition, the manner in which an RCM responds to the atmospheric forcing provided by a GCM can be region specific
79 (Rana et al., 2020; Wu and Gao, 2020) (e.g., regions located in close proximity to the boundaries of the RCM domain
80 can be more severely affected by the driving GCMs, than regions at the center of the RCM domain or there can be
81 region specific response around complex topography versus lowlands). Also, the degree to which an RCM is
82 influenced by the driving GCM can be process specific. For instance, when there is a strong large-scale circulation
83 signal that is introduced to an RCM domain (e.g. advective mid-latitude storms), it is likely that the RCM will be able
84 to reproduce the information that is received at its lateral boundaries, however, the GCM's impact on the RCM
85 simulation may also vary depending on how far a region lies from the RCM domain boundaries (Kim et al., 2020). If,
86 however, the large-scale forcing is weak, then the atmospheric conditions simulated within the RCM domain are more
87 dependent on the dynamic and thermodynamic processes employed by the RCM (e.g. convective thunderstorms).
88 In this work we aim to assess whether it is the RCMs or their driving GCMs that dominate monthly precipitation
89 climatology, monthly precipitation bias and climate change signal over SAF. We take into account the region-specific
90 characteristics of this question by analyzing SAF and three subregions, namely southeastern Angola, Mozambique,
91 and South Africa. We also consider the different atmospheric processes that are at play over each region by analyzing
92 monthly climatologies. Precipitation over SAF results from various atmospheric processes that are highly variable
93 during the rainy season (Oct-Mar), so by performing the analysis on a monthly basis, we are able to indirectly study
94 how certain processes are reproduced by GCM and RCM simulations. In order to differentiate between the signal
95 emanating from the RCMs and that emanating from their driving GCMs, we use the analysis of variance (ANOVA)
96 in both the GCM and the RCM ensembles (Déqué et al., 2007, 2012). Since the information provided by RCMs will
97 eventually be used by both climate and non-climate scientists, especially in light of climate change impact studies, we
98 aim to provide some information with regards to how much each RCM is affected by its driving GCM and what
99 climate change signals are consistent in both RCMs and GCMs.

100

101 **2 Material and methods**

102 **2.1 Data**

103 The data analyzed in the current work consist of RCM simulations performed in the context of CORDEX-Africa, a
104 set of simulations performed in the context of CMIP5, the CHIRPS satellite rainfall product (Funk et al., 2015), the
105 ERA5 reanalysis dataset (Hersbach et al., 2020), the CRU gridded observational dataset (Harris et al., 2020), and the
106 MSWEP precipitation product (Beck et al., 2019). More specifically, the CORDEX-Africa simulations selected are
107 those that were driven by more than two GCMs (at least three simulations available using the same RCM driven by at
108 least three different GCMs) and for which there are runs available for both the historical and the future period under
109 RCP8.5. All RCMs employed a relaxation zone which was either 10 grid-points wide (CCLM4-8-17.v1) or eight
110 points wide (RCA4.v1 and REMO2009.v1). Relaxation in all RCM simulations was performed using Davie's method

111 (Davies, 1976, 1983). The CMIP5 GCMs selected are the ones that were used to drive the CORDEX-Africa
 112 simulations. All RCM and GCM simulations were retrieved from the Earth System Grid Federation. The CHIRPS
 113 rainfall product is used for calculating precipitation biases in both the CORDEX-Africa and CMIP5 ensembles..
 114 CHIRPS is available at 5 km spatial resolution and for the calculation of biases it was remapped to the coarser
 115 resolution grid using conservative remapping. A fact that is commonly obscured is that observational datasets are
 116 often considered as “ground truth” however, they are also subject to multiple sources of uncertainty, caused by the
 117 underlying station datasets used, the statistical algorithms employed in spatial interpolation methods or the algorithms
 118 employed in satellite rainfall products (Le Coz and van de Giesen, 2020). More specifically, over southern Africa, it
 119 was found that gauge-based products employing spatial interpolation methods displayed high uncertainty over regions
 120 where the underlying station network was scarce, mainly over the Angola region and the northern parts of SAF
 121 (Karypidou et al., 2022). In addition, it was found that this attribute was inherited by all rainfall satellite products that
 122 were using direct merging techniques with gauge-based datasets. Here, we display monthly precipitation during the
 123 historical period (1985-2005) across four observational datasets, given in **Table 1**. More specifically, we use the
 124 CRUv4.06 dataset (Harris et al., 2020), which is a purely gauge-based product (employing station data and a spatial
 125 interpolation algorithm to provide a spatially continuous gridded product), ERA5 (Hersbach et al., 2020), which is a
 126 reanalysis product, CHIRPS (Funk et al., 2015), which is a satellite rainfall product, and finally, MSWEP (Beck et al.,
 127 2017) which is a product merging station data, satellite data and dynamic model outputs. All datasets have been
 128 analyzed using monthly mean values. The results are displayed in **Fig. 1**. As shown, there is a substantial agreement
 129 among them, both with regards to the spatial and temporal pattern of monthly precipitation over southern Africa.
 130

131 Table 1 Gauge-based, satellite, reanalysis and merged precipitation products analyzed over the study region using
 132 monthly mean precipitation for the period 1985-2005.

Dataset	Resolution	Frequency	Type	Period
CRU TS4.06	0.5°	Monthly total	Gauge-Based	1901-2021
MSWEP	0.1°	3-hourly	Merged product	1979-present
CHIRPS.v2	0.05°	Daily totals	Satellite	1981-present
ERA5	~0.25°	Hourly	Reanalysis	1979-present

133
 134 Our analysis is split into two sections: the qualitative and the quantitative part. In the qualitative part, we aim to
 135 identify if RCMs exhibit systematic behavior relative to their driving GCMs. For the quantitative part, we aim to
 136 quantify the degree to which monthly precipitation climatologies, biases and climate change signals are affected by
 137 the RCMs or by the driving GCMs. For this purpose, we employ an ensemble of 19 RCM simulations driven by 10
 138 GCMs and the driving GCMs that were used to provide the lateral boundary conditions to the RCMs. From the
 139 historical simulations we use the period 1985-2005 and from the projection simulations we use the period 2065-2095
 140 under RCP8.5. All CORDEX-Africa simulations are available at ~50 km horizontal resolution and are shown in **Table**
 141 **2**, while the horizontal resolution for the driving GCMs is provided in **Table 3**.

142
 143 **Table 2** Input RCM and GCM simulations used. The CORDEX-Africa simulations are given in the columns. The
 144 CMIP5 GCMs used as driving fields are given in the rows.

	CCLM4-8-17.v1	RCA4.v1	REMO2009.v1
--	----------------------	----------------	--------------------

CanESM2		√	
CNRM-CM5	√	√	
EC-EARTH	√	√	√
HadGEM2-ES	√	√	√
MIROC5		√	√
MPI-ESM-LR	√	√	√
IPSL-CM5A-LR			√
IPSL-CM5A-MR		√	
CSIRO-Mk3-6-0		√	
GFDL-ESM2M		√	
NorESM1-M		√	

145

146 **Table 3** Horizontal resolution of the CMIP5 GCMs used as driving fields in the CORDEX-Africa simulations.

GCMs	Latitude Res.	Longitude Res.	References
CanESM2	2.7906 °	2.8125 °	(CCCma, 2017)
CNRM-CM5	1.40008 °	1.40625 °	(Voltaire et al., 2013)
CSIRO-Mk3-6-0	1.8653 °	1.875 °	(Jeffrey et al., 2013)
EC-EARTH	1.1215 °	1.125 °	(Hazeleger et al., 2010)
GFDL-ESM-2M	2.0225 °	2.5 °	(Dunne et al., 2012)
HadGEM2-ES	1.25 °	1.875 °	(Collins et al., 2011)
IPSL-CM5A-MR	1.2676 °	2.5 °	(Dufresne et al., 2013)
IPSL-CM5A-LR	1.894737 °	3.75 °	
MIROC5	1.4008 °	1.40625 °	(Watanabe et al., 2010)
MPI-ESM-LR	1.8653 °	1.875 °	(Giorgetta et al., 2013)
NorESM1-M	1.894737 °	2.5 °	(Bentsen et al., 2013)

147

148 **2.2 Methods**

149 The study region and subregions considered are depicted in **Fig. 2**. The subregions are selected based on particular
150 phenomena and processes that are of importance for the seasonal cycle of precipitation. More specifically, Region A
151 (hereafter: SAF-All) encompasses the entire SAF region and is defined as the area extending from 10 °E to 42 °E and
152 from 10 °S to 35 °S. Region B (hereafter: Angola region) was selected to capture the main region of interest with
153 regards to the Angola Low (AL) pressure system (Howard and Washington, 2018) and covers the area extending from
154 14 °E to 25 °E and from 11 °S to 19 °S. Region C (hereafter: East Coast) covers the eastern coastline, Mozambique and
155 parts of the surrounding countries and extends from 31 °E to 41 °E and from 10 °S to 28 °S. Lastly, we define the SAfr
156 region, which covers much of South Africa and extends from 15 °E to 33 °E and from 26 °S to 35 °S.

157 One of the primary synoptic scale features controlling precipitation over SAF is the Angola Low (AL) pressure system
158 (Reason and Jagadheesha, 2005; Lyon and Mason, 2007; Crétat et al., 2019; Munday and Washington, 2017; Howard
159 and Washington, 2018), which has a distinct seasonal cycle throughout the rainy season (Oct-Mar). This motivates its
160 selection as a subregion for our study. The AL exhibits heat low characteristics during Oct-Nov and tropical low
161 characteristics during Dec-Feb (Howard and Washington, 2018). This suggests that during Oct-Nov, since

162 precipitation is thermally induced and thus tightly dependent on land-atmosphere interactions, it will be the RCMs
 163 that are dominant in controlling precipitation processes. As the rainy season progresses, the AL changes to a tropical
 164 low pressure system and its formation is controlled by the large-scale circulation that is characterized by easterly
 165 winds from the Indian Ocean that enter SAF via the Mozambique Channel. Since precipitation during Dec-Feb is
 166 caused by the tropical low phase of the Angola Low pressure system, which is the monthly aggregate of frequent
 167 transient low pressure systems crossing southern African (Munday and Washington, 2017; Howard and Washington,
 168 2018; Howard et al., 2019), we hypothesize that the impact of the driving GCMs during Dec-Feb is enhanced.
 169 In addition, the wider area of Mozambique is a region where the majority of tropical cyclones/depressions make
 170 landfall over continental SAF. The occurrence of transient low-pressure systems is enhanced during the core of the
 171 rainy season (Dec-Feb) and thus we are interested in identifying whether the impact of the driving GCMs is dominant
 172 during Dec-Feb. Also, since according to Muthige et al. (2018), the number of landfalling tropical cyclones under
 173 RCP8.5 is expected to decline in the future, we are interested in examining whether the impact of the driving GCMs
 174 to the RCM simulations will be altered under future conditions. Hence, the East Coast region is used as a region
 175 indicative of the landfalling tropical cyclones/depressions. Lastly, we examine the area encompassing South Africa
 176 (hereafter: SAfr) due to its strong land-ocean gradients, complex topography and strong seasonal variations in rainfall
 177 zones.

178

179 **2.2.1 Monthly precipitation climatology and bias**

180 In order to assess whether or not the RCMs improve the monthly precipitation climatologies relative to their driving
 181 GCMs, we employ a method initially described in Kerkhoff et al. (2015) and later employed by Sørland et al. (2018),
 182 which displays in a scatterplot form the RCM increment as a function of the GCM bias. More specifically, the RCM
 183 increment is described as the difference of each RCM simulation from its driving GCM (RCM-GCM). The RCM
 184 increment is plotted against the GCM bias (GCM-OBS). This plot displays whether or not the RCM increment
 185 counteracts the GCM bias. If the RCM increment reduces the GCM bias, then points are expected to lie along the $y=-$
 186 x line (negative correlation). On the contrary, if the RCM increment increases the GCM bias, then points are expected
 187 to lie along the $y=x$ line (positive correlation). If the RCM increment and the GCM bias are independent, then points
 188 are expected to be scattered randomly.

189

190 **2.2.2 Climate change signal**

191 The climate change signal (CCS) is identified as the monthly mean difference between the future period (2065-2095)
 192 minus the historical period (1985-2005). As an exploratory method of inspecting the differences between each RCM
 193 simulation from its respective driving (GCM) for monthly precipitation during both the historical and the future period,
 194 we subtract the downscaled precipitation field (RCM_{DRI}) from its driving (DRI) GCM, as in **Eq. 1**:

$$DIFF = RCM_{DRI} - DRI \quad \text{Eq. 1}$$

195 If $DIFF > 0$ (monthly precipitation), then we assume that the RCM enhances precipitation, relative to its driving GCM,
 196 while if $DIFF < 0$ then we assume that the RCM reduces precipitation, relative to its driving GCM. This method is
 197 employed in the qualitative part of the analysis.

198

199 2.2.3 Analysis of variance

200 Additionally, we employ an ANOVA decomposition (Déqué et al., 2007, 2012), in order to understand whether it is
201 the RCMs or their respective driving GCMs that are responsible for controlling precipitation over the historical (1985-
202 2005) period and the future period (2065-2095). For this purpose, we use two quantities, namely the “inter-RCM”
203 variance and the “inter-GCM” variance, as in Déqué et al. (2012). More specifically, the “inter-RCM variance” is the
204 variance between all the RCM simulations that are driven by the same GCM. Subsequently, all variances obtained for
205 all driving GCMs are averaged.

$$RCM_{var} = \frac{1}{N_{RCM}} \sum_{RCM_j} (P_j - \bar{P}_j)^2 \quad \text{Eq. 2}$$

206 The quantity P_j is the monthly precipitation obtained from all RCMs (j) that were driven by the same GCM. The
207 quantity \bar{P}_j is the mean monthly precipitation obtained by all RCMs (j) that share a common driving GCM. As a final
208 step, the average of all variances is calculated.

$$Inter_RCMvar = \frac{\sum GCM_j}{N} \quad \text{Eq. 3}$$

209 Similarly, the “inter-GCM” variance describes the variance between all the GCMs that were used to drive a single
210 RCM and then averaged over all the variances obtained for all driven RCMs. N refers to all available simulations
211 contributing to either the inter-RCM or inter-GCM variance.

$$GCM_{var} = \frac{1}{N_{GCM}} \sum_{GCM_i} (P_i - \bar{P}_i)^2 \quad \text{Eq. 4}$$

212 Likewise, the average of all variances is calculated.

$$Inter_GCMvar = \frac{\sum RCM_i}{N} \quad \text{Eq. 5}$$

213 Both “inter-RCM” and “inter-GCM” variances are normalized by the total variance obtained for all months, as in
214 (Vautard et al., 2020), so that all values, both for historical and projection runs and RCM and GCM simulations are
215 comparable. A schematic of the process described above is provided in **Fig. S1**.

216 3 Results

217 The October and January precipitation climatologies for the period 1985-2005 are displayed in **Fig. 3** and **Fig. 4**,
218 respectively. We use October and January climatologies, because these two months may be considered representative
219 of the distinctive processes controlling precipitation over SAF (see section 2.2). We avoid using seasonal means, since
220 the temporal averaging of precipitation often obscures attributes that are better identified on a monthly level. The
221 remaining months of the rainy season are shown in the supplementary material. More specifically, we use October as
222 it is the month that heralds the onset of the rainy season and is often associated with weak precipitation and convective
223 processes that are mainly due to excess surface heating. Also, it is during October that the most intense formations of
224 the heat low expression of the AL are observed. Likewise, we use January as it represents the core of the rainy season,
225 with very strong large-scale precipitation, mainly from the southeastern (SE) part of SAF, through transient synoptic
226 scale low pressure systems.

227 As it is displayed in **Fig. 3**, precipitation during October occurs in the northwestern (NW) part and the SE part of SAF.
228 Precipitation in the NW part is associated with the southward migration of the rainband (Nicholson, 2018), while
229 precipitation over the SE part is associated with an early formation of the tropical temperate troughs (TTTs). As it is
230 evident from **Fig. 3**, CCLM4-8-17.v1 reduces precipitation amounts (approximately 4-5 mm/d) in both the NW and
231 SE parts of SAF, relative to the lateral boundary forcing it receives. On the contrary, RCA4.v1 systematically enhances
232 precipitation amounts, regardless of the driving GCM. Also, precipitation according to RCA4.v1 displays a very
233 localized spatial pattern with very strong spatial heterogeneity. This attribute is indicative of specific structural model
234 biases related to how high-resolution elevation affects precipitation in RCA.v1 (Van Vooren et al., 2019). This is
235 particularly evident in the mountainous region over coastal Angola. REMO2009.v1 also enhances precipitation
236 amounts regardless of the driving GCM, however in a much more spatially homogeneous way than RCA4.v1.

237
238 As it is shown in **Fig. 4**, high precipitation amounts during January are observed over the northern and eastern regions
239 of SAF. During January, differences among the driving GCMs become more pronounced, however, all models agree
240 on the dry conditions observed over the southwestern (SW) part of SAF. With regards to the downscaled products,
241 CCLM4-8-17.v1 produces high precipitation amounts over the central part of northern SAF but displays varying
242 amounts of precipitation over the coastal parts, depending on the driving GCM. RCA4.v1 downscales precipitation in
243 a very localized pattern and enhances precipitation over areas with steep terrain. Also, precipitation over the lake
244 Malawi region is particularly enhanced, regardless of the driving GCM. REMO2009.v1 displays similar precipitation
245 amounts to its driving GCMs, however it enhances precipitation over the coastal part of Angola and Mozambique and
246 yields excess precipitation over lake Malawi, when it is driven by HadGEM2-ES and IPSL. The monthly climatologies
247 for the rest of the rainy season months are shown in the supplementary material (**Fig. S2 – S5**).

248
249 In **Fig. 5** the monthly precipitation bias for October over SAF is shown. Biases are calculated using the CHIRPS
250 satellite rainfall product as a reference. With the exception of IPSL-CM5A (LR/MR) and CanESM2, all other GCMs
251 display a consistent wet bias that ranges from 0.1 – 30 mm/d (in isolated areas), with most values over SAF falling
252 between 0.1 to 3 mm/d. Overall, the same pattern generally holds for RCA4.v1 and REMO2009.v1, while CCLM4-
253 7-18.v1 displays a systematic dry bias that reaches 2 mm/d, when forced with EC-EARTH, MPI-ESM-LR and
254 HadGEM2-ES. More specifically, concerning RCA4.v1, the region where the highest wet bias is observed is over the
255 Angola region and over the NW parts of coastal Angola. The dry bias regions in RCA4.v1 are identified over the
256 northeastern (NE) and southern parts of SAF and they rarely exceed -1.5 mm/d.

257 The monthly precipitation biases for January over SAF are shown in **Fig. 6**. There is a prevailing wet bias identified
258 in almost all GCMs that typically reaches 3 - 3.5 mm/d, however, in MIROC5, NorESM and GFDL-ESM2M the
259 biases exceed 5 mm/d over a major part of SAF. Another feature that systematically appears in GCMs is a dry bias
260 over the NE part of SAF. This bias pattern is also identified in almost all RCMs with a systematic wet bias over central
261 and western SAF and a region of dry bias in the NE part. More specifically, in RCA4.v1 and REMO2009.v1, there is
262 a dry bias over the NE and the southern coast of SAF, while in CCLM4-7-18.v1 the dry bias over the eastern region
263 extends inland to cover almost the whole of Mozambique. Another interesting feature is identified around the Angolan

264 coast, where wet biases exceed 5 mm/d, while over an adjacent region there is a strip of dry biases that reaches 2
265 mm/d. Considering the abrupt increase in elevation and the steep escarpment over the coastal Angola-Namibia region,
266 this is possibly caused by local circulation driving excess moisture transport from the Atlantic Ocean and overly
267 aggressive orographically triggered precipitation on the windward side of the topography (wet bias strip), that leads
268 to dry conditions in the lee side (dry bias strip) (Howard and Washington, 2018). It is noted that the wet bias over the
269 coastal region is identified in most of the RCA4.v1 simulations and in all REMO2009.v1 simulations, however, the
270 dry bias in the lee side is seen in CCLM4-7.18.v1 only. The monthly precipitation biases for the rest of the rainy
271 season months are shown in the supplementary material (**Fig. S6 – S9**). Monthly precipitation biases averaged over
272 southern Africa (SAF-All) and the three subregions examined are displayed in **Fig. S10**.

273
274 A more detailed look into specific subregions over SAF where certain climatological features and processes are at
275 play, can help gain a more in-depth insight of how the precipitation biases are distributed during each month of the
276 rainy season and whether or not the RCMs display any improvement relative to their driving GCMs. For this reason,
277 we plot the RCM increments (RCM-GCM) as a function of the GCM biases (GCM-OBS). The results for October
278 over SAF and the three subregions are displayed in **Fig. 7**. In general, all points are identified close to the $y=-x$ line,
279 hence there is a tendency that RCMs systematically counteract GCM biases. There are nonetheless substantial
280 differences between the four regions. For instance, over SAF-All region the IPSL-MR GCM has a wet bias equal to
281 almost 1 mm/day, which is counteracted by RCA by an increment of -0.4 mm/month. Other RCA simulations when
282 driven by HadGEM2-ES, CNRM-CM5 or EC-EARTH, display an RCM increment similar to that of the GCM bias,
283 hence RCMs mitigate the GCM bias. Over the Angola region most of the RCMs display an RCM increment that is
284 nearly equal to the GCM bias. Similar conclusions are drawn for the East Coast and the South Africa regions. The
285 RCM increments as a function of the GCM biases for January are shown in **Fig. 8**. For all regions except of the SAfr
286 region points are lying closely to the $y=-x$ line, hence overall, RCM increments counteract the GCM biases. The
287 scatterplots for the rest of the months of the rainy season are shown in the supplementary material (**Fig. S11 – S14**).
288 In general, although precipitation in RCMs is strongly dependent on the driving GCMs, the RCM increments are
289 anticorrelated to the GCM biases. The anticorrelations are particularly strong for the Dec-Mar period of the rainy
290 season over SAF-All region and the Angola and East Coast subregions,, but not over the SAfr subregion (**Fig. S15**).

291 In **Fig. 9** the analysis of variance of all RCMs driven by the same GCM and of all GCMs driving the same RCM is
292 shown. Values are spatially averaged for southern Africa and the three subregions examined (land grid points only)
293 and refer to the period 1985-2005. In the SAF-All region, monthly precipitation during October and November is
294 dominated by the RCMs, while during Jan-Mar, it is the GCMs that play a dominant role in formulating precipitation
295 over SAF. This is indicative of the impact that RCMs exert on the formulation of precipitation during Oct-Nov-Dec
296 and the fact that the contribution from the GCMs becomes secondary during Jan-Feb-Mar. The fact that the
297 contribution of RCMs during Oct-Nov-Dec dominates can be attributed to the fact that precipitation during these
298 months is the result of regional processes that are largely dependent on the coupling between the surface and the
299 atmosphere. The land-atmosphere coupling is a characteristic resolved by the RCMs, through mechanisms simulated

300 by land surface models, planetary boundary layer schemes, convection schemes etc., making the contribution of the
301 large scale drivers from the GCM less important. However, during Jan-Feb-Mar we observe that the contribution from
302 the RCMs is reduced, and it is the GCMs that control the monthly precipitation variability. This can be attributed to
303 the fact that during Jan-Feb-Mar it is the large-scale circulation that modulates precipitation over SAF and the GCMs
304 control the transient synoptic scale systems that enter SAF. Over the Angola region, the pattern is similar, however,
305 October and November precipitation is closer to the diagonal, indicating an almost equal contribution by both RCMs
306 and GCMs. While, Dec-Feb move closer to the diagonal, precipitation during March is mainly formulated by GCMs.
307 Over the East Coast region, October remains equally influenced by both RCMs and GCMs, however November and
308 December are dominated by the influence of the RCMs. Over the SAfr region, precipitation for all months except
309 October is influenced by GCMs.

310 In **Fig. 10** the climate change signal for October precipitation over SAF is depicted. All GCMs agree that October
311 precipitation will decline by approximately 2 mm/d over the regions that experience precipitation during this period,
312 namely the NW and SE parts of SAF. In addition, some GCMs display a minor precipitation increase (0 - 0.5 mm/d)
313 over the SW part of SAF, while some others display a slightly larger (1.5 mm/d) precipitation increase over the eastern
314 parts of South Africa. Moreover, it is seen that the precipitation change signal is replicated by almost all the
315 downscaling RCMs, nevertheless, there are some considerable differences between the RCMs and their driving GCM.
316 More specifically, RCA4.v1 in almost all simulations, displays a larger reduction of the precipitation change signal
317 relative to its driving GCM, both in magnitude and in spatial extent. Precipitation changes in CCLM4-8-17.v1 seem
318 to follow closely the driving GCMs, with a severe exception when CNRM-CM5 is used (the NW part of SAF
319 experiences precipitation decline almost 4 mm/d larger than in the driving GCM). The case for when CCLM4-8-17.v1
320 is driven by CNRM-CM5 may be partly caused by the fact that the historical simulation had erroneously used lateral
321 boundary conditions from a different simulation member of CNRM-CM5 (Vautard et al., 2020). In REMO2009.v1, a
322 precipitation decline region is identified in the NW part of SAF and a minor precipitation increase over eastern South
323 Africa is identified. This pattern for REMO2009.v1 appears to be consistent, regardless of the driving GCM, which
324 could be partly explained by the fact that precipitation during October is thermally driven, and thus the impact of the
325 driving GCMs is not dominant. The precipitation increase in the SE part of SAF is seen over a localized region and
326 could be associated with an increase in the precipitation caused by the Tropical Temperate Troughs (TTTs) (Ratna et
327 al., 2013; Macron et al., 2014; Shongwe et al., 2015).

328 In **Fig. 11** the climate change signal for precipitation during January is displayed. The precipitation change displays a
329 very strong regional heterogeneity. It is also observed that although there is a strong precipitation change signal in all
330 driving GCMs, not all RCMs downscale the signal uniformly. It is also notable that, even among the GCMs, there are
331 substantial differences in the spatial extent and sign of the change. Nevertheless, there are some features that appear
332 in most of the simulations. For instance, almost all GCMs project drying conditions over the SW part of SAF,
333 especially the coastal zone. The precipitation decline is equal to -1 mm/d. This could be explained by a consistent
334 increase in frequency of the Benguela Coastal Low-Level Jet events (Lima et al., 2019; Reboita et al., 2019), causing
335 oceanic upwelling and a subsequent reduction in precipitation. In addition, there is a subset of GCMs that identify a

336 severe precipitation decline over the Angola region that reaches -5 mm/d. Furthermore, in many GCMs a region of
337 precipitation increase is identified, extending from central SAF towards SE SAF. This is particularly identifiable in
338 HadGEM2-ES, and the RCM simulations forced by it. The monthly precipitation changes for the rest of the rainy
339 season months is shown in the supplementary material (**Fig. S16 – S19**).

340 In **Fig. 12** the spatial average of the $RCM_{DRI} - DRI$ difference (DIFF) is shown for the whole of SAF (land grid points
341 only). If $DIFF > 0$, it indicates that the RCMs enhance precipitation relative to their driving GCM, while if $DIFF < 0$
342 then RCMs reduce precipitation relative to their driving GCM. As it is shown, DIFF values for October are symmetric
343 around zero and do not exceed the range $(-1) - 1$ mm/d, either for the historical or the future period. Almost symmetric
344 are the DIFF values for November also, however, their spread increases, reaching values that range $(-2) - 2$ mm/d.
345 During both months, CCLM4-7-18.v1 always reduces precipitation amounts relative to the lateral boundary forcing it
346 receives, regardless of the driving GCM or the period examined. During December, the precipitation reduction in all
347 RCMs becomes more pronounced and reaches values equal to -3 mm/d. In January, only one RCM enhances
348 precipitation (~ 0.5 mm/d) with all the rest displaying precipitation reduction. During February and March, some
349 positive DIFF values re-appear for some simulations. Overall, there is a strong linear relationship between DIFF in
350 1985-2005 and 2065-2095, which further implies that if an RCM is drier than its driving GCM during the historical
351 period, then it will retain this attribute during the future period also. Nonetheless, we highlight that RCMs preserve
352 precipitation change signal generated by the GCMs. Considering that one primary shortcoming of the GCMs over
353 SAF is their wet bias and that RCMs systematically reduce this bias, we gain increased confidence that RCMs can be
354 reliably used for assessments of future precipitation change.

355 In **Fig. 13** the spatial average of the precipitation change signal from RCMs and their driving GCMs relative to 1985-
356 2005 for SAF and the three subregions is displayed. Concerning SAF-All region, all models during October identify
357 a precipitation reduction at the end of the 21st century that can reach -0.9 mm/d. The precipitation decline signal is
358 also identified during November, indicating a later onset of the rainy season over SAF, as it has already been shown
359 for CMIP5 (Dunning et al., 2018). During December and January there is a variability in the spatial averages of the
360 change signal that ranges from -0.8 to 0.8 mm/d. A similar pattern is also seen for February and March. The distribution
361 of the ensemble members for both RCMs and GCMs over the Angola and the East Coast subregions is similar to that
362 of SAF-All region, however over the Angola and the East Coast subregions precipitation change values display a
363 considerably larger spread. Over the SAfr region the climate change signal is symmetric around 0 for all months,
364 except March.

365 The impact of the RCMs and GCMs on monthly precipitation for the period 2065-2095 under RCP8.5 is shown in
366 **Fig. 14**. The SAF-all region and the Angola subregion show a similar behavior as in the historical period (**Fig. 9**),
367 however, over the East Coast subregion, precipitation during March is more strongly dominated by GCMs. The same
368 observation holds also over the SAfr subregion. In general, regional processes continue to dominate contributions to
369 variability during Oct-Nov, while large scale features dominate during Dec-Mar.

370

371 **3 Discussion and conclusions**

372 In this work we investigate whether it is the RCMs or the driving GCMs that control the monthly precipitation
373 variability, monthly precipitation biases and the climate change signal over southern Africa and how these
374 relationships vary from month-to-month throughout the rainy season. Our work examines monthly precipitation
375 variance caused by the lateral boundary conditions and does not examine parameter and structural uncertainty
376 separately in the multi-RCM and the multi-GCM ensembles analyzed. More specifically, we use an ensemble of 19
377 RCM simulations performed in the context of CORDEX-Africa and their driving GCMs. According to the literature
378 (Munday and Washington, 2018), precipitation in the CMIP5 simulations is characterized by a systematic wet bias
379 over southern Africa. In the CORDEX-Africa RCM simulations there is also a persistent wet bias, especially during
380 the core of the rainy season (DJF), however, it is of smaller magnitude and of smaller spatial extent. It is found that
381 RCMs reduce monthly precipitation compared to their driving GCMs for both historical (1985-2005) and future
382 periods (2065-2095) under RCP8.5.

383 The Angola region, which encompasses the activity of the Angola Low pressure system, displays the highest wet
384 biases with regards to mean monthly precipitation, among all subregions examined. The month with the largest wet
385 biases (for the Angola region) is found to be November, while the month with the largest precipitation bias spread is
386 found to be March. In all months except October, the CMIP5 GCMs display biases that are approximately 1 - 1.5
387 mm/d wetter than the wettest CORDEX-Africa RCM ensemble members. Over the East Coast region, representing
388 the wider area over Mozambique, the bias signal is reversed after January, with most of the RCMs displaying a dry
389 bias. Over the SAfr region, the majority of models display a consistent wet bias for all months of the rainy season. All
390 models (CMIP5 and CORDEX-Africa) display an intense dry bias in the NE part of SAF, which can be related to the
391 misrepresentation of the moisture transport entering the region from the Indian Ocean (Munday and Washington,
392 2018). In general, although RCMs display an improvement of precipitation biases relative to their driving GCMs, still
393 some bias patterns persist even in RCMs, calling for a process-based evaluation of specific climatological features
394 such as the formulation of the Angola Low and the transport of moisture from the NE part of SAF towards central
395 SAF.

396 More specifically, we found that CCLM4-7-18.v1 produces the smallest bias when the whole of SAF is examined,
397 however, it displays a systematic dry bias over the East Coast region (greater Mozambique region), hence, CCLM4-
398 7-18.v1 should be used with caution over eastern SAF, especially if it is exploited within drought-related climate
399 services. Concerning RCA4.v1, we find a very regionally heterogeneous -almost pixelated- spatial pattern for
400 precipitation, which can be attributed to the sharp topography used (Van Vooren et al., 2019). RCA4.v1, due to the
401 large size of its ensemble, is optimal for analyzing its behavior under different driving GCMs. In general, we find that
402 RCA4.v1 is more prone to follow the signal received from the driving GCMs, contrary to what is observed for
403 CCLM4-7-18.v1. REMO2009.v1 presents a compromise between the behaviors of RCA4.v1 and CCLM4-7-18.v1.

404 It is highly recommended that when RCM simulations are used for the whole of SAF or a subregion thereof, the spread
405 and statistical properties of all available RCMs and their driving GCMs should be examined and an ensemble of RCMs
406 should be employed based on their ability to reproduce key climatic features of the region of interest. Increasing

407 evidence is provided that not all models are fit for constructing an ensemble mean (or median) for all regions (Her et
408 al., 2019; Raju and Kumar, 2020; Tebaldi and Knutti, 2007). Lastly, a very important aspect when the calculation and
409 characterization of biases is discussed for GCMs and RCMs, is that biases are assessed based on a satellite or gauge-
410 based product, which are often erroneously regarded as “the ground truth” (Harrison et al., 2019; Alexander et al.,
411 2020). Of course, the climate community is bound to work with the state-of-the-science products that are available,
412 however, biases and errors in the “observational datasets” should be kept in mind when the bias of climate models is
413 discussed. In this work we use the CHIRPS precipitation product, as it has been shown to outperform other satellite
414 precipitation products (Toté et al., 2015; Ayehu et al., 2018; Dinku et al., 2018).

415 Concerning the climate change signal, there is a strong agreement among all GCMs and RCMs that precipitation
416 during October will decrease by $(-0.1) - (-1)$ mm/d, a fact associated with a projected later onset of the rainy season,
417 which is further linked with a northward shift of the tropical rain belt (Dunning et al., 2018; Lazenby et al., 2018).
418 The topic of reduced early rainfall over southern Africa for the end of the 21st century under all emission
419 scenarios/pathways has been examined extensively for the CMIP3 and CMIP5 GCM ensembles (Seth et al., 2011;
420 Cook and Vizu, 2021; Lazenby et al., 2018; Howard and Washington, 2019). A common observation in all CMIP5
421 GCMs for the early rainy season by the end of the 21st century is that instability over southern Africa reduces, surface
422 temperature increases, and the heat low phase of the Angola Low pressure system is strengthened (Howard and
423 Washington, 2019). However, rainfall decline in the CMIP5 ensemble over southern Africa should be additionally
424 considered in the context of the systematic precipitation biases already diagnosed in the historical simulations
425 (Munday and Washington, 2018; Howard and Washington, 2019). Considering that the systematic wet precipitation
426 bias is significantly reduced in the CORDEX-Africa ensemble relative to their driving CMIP5 GCMs (Karypidou et
427 al., 2022b), we gain confidence that future precipitation projections according to the CORDEX-Africa ensemble
428 provide a more plausible future scenario. For the rest of the months, the results are variable, indicating the need for a
429 multi-model approach, when climate change impacts are assessed. A feature that is identified in some GCMs and is
430 transferred to the downscaling RCMs, is a precipitation increase that extends from the central SAF region towards the
431 southeast. This result is consistent with previous work that shows an increase in frequency of landfalling cyclones
432 along the eastern seaboard of SAF (Muthige et al., 2018). Since tropical cyclones are a particular cause of severe
433 flooding events over Mozambique, there is an urgent need for planning and mitigation strategies in the region.

434 Concerning precipitation variability and whether it is the RCMs or the driving GCMs that dominate monthly
435 precipitation, we find that, as expected, over the whole of SAF (SAF-All region), October and November are
436 dominated by RCMs, while during Dec-Mar it is the GCMs that mainly formulate the precipitation climatologies. This
437 is explained by the fact that after December there is a strong large-scale forcing, which is provided to the RCMs by
438 the lateral boundary conditions given through the GCMs. The results for the historical period are comparable to that
439 for future projections.

440 Lastly, it is imperative to highlight that the impact of the lateral boundary conditions on RCM simulations comprise
441 only a portion of the potential sources of uncertainty in the CORDEX-Africa ensemble examined, therefore attributing
442 entirely the variance of RCM simulations to the driving GCMs would be erroneous. Therefore, we mention that
443 uncertainty in RCM simulations can have a plethora of sources that are mainly categorized as parameter or structural

444 uncertainty (Günther et al., 2020; Howland et al., 2022). These types of uncertainty sources may relate to the
445 parameterization schemes employed by each RCM or assumptions and numerical choices involved in the dynamics
446 of each specific RCM. However, since within CORDEX-Africa only a limited number of variables is being made
447 available to the community, it would be impossible to meticulously comment on all possible sources of uncertainty
448 and assess the impact of their variance on monthly precipitation.

449 *Code and data availability*

450 For the data processing and statistical analysis we used the R Project for Statistical Computing ([https://www.r-](https://www.r-project.org/)
451 [project.org/](https://www.r-project.org/)), the Climate Data Operators (CDO) (<https://code.mpimet.mpg.de/projects/cdo/>) and Bash programming
452 routines. Processing scripts are available via ZENODO under DOI: <https://doi.org/10.5281/zenodo.5569984>. CMIP5
453 and CORDEX-Africa precipitation data were retrieved from the Earth System Grid Federation (ESGF) portal
454 (<https://esgf-data.dkrz.de/projects/esgf-dkrz/>). The Climate Hazards Group InfraRed Precipitation with Station data
455 (CHIRPS) products were retrieved from: <https://www.chc.ucsb.edu/data/chirps>.

456

457 *Supplement*

458 The supplement related to this article is available online.

459

460 *Author contribution*

461 MCK, SPS and EK designed the research. MCK performed the analysis and prepared the manuscript. SPS, EK, LS
462 and GN edited the manuscript and provided corrections.

463

464 *Competing interests*

465 The authors declare that they have no competing interests.

466

467 *Acknowledgements*

468 This article is funded by the AfriCultuReS project "Enhancing Food Security in African Agricultural Systems with
469 the Support of Remote Sensing", (European Union's Horizon 2020 Research and Innovation Framework Programme
470 under grant agreement No. 774652). The authors would like to thank the Scientific Support Centre of the Aristotle
471 University of Thessaloniki (Greece) for providing computational/storage infrastructure and technical support. MCK
472 was funded by the Hellenic Foundation for Research & Innovations, under the 2nd Call for PhD Candidates (application
473 No. 1323). This work is dedicated to the beautiful memory of Ms Anatoli Karypidou.

474

475 **References**

476 Beck, H. E., Vergopolan, N., Pan, M., Levizzani, V., van Dijk, A. I. J. M., Weedon, G. P., Brocca, L., Pappenberger, F.,
477 Huffman, G. J., and Wood, E. F.: Global-scale evaluation of 22 precipitation datasets using gauge observations and
478 hydrological modeling, *Hydrol. Earth Syst. Sci.*, 21, 6201–6217, <https://doi.org/10.5194/hess-21-6201-2017>, 2017.

479 Beck, H. E., Wood, E. F., Pan, M., Fisher, C. K., Miralles, D. G., Dijk, A. I. J. M. van, McVicar, T. R., and Adler, R. F.: MSWEP
480 V2 Global 3-Hourly 0.1° Precipitation: Methodology and Quantitative Assessment, *Bull. Am. Meteorol. Soc.*, 100,
481 473–500, <https://doi.org/10.1175/BAMS-D-17-0138.1>, 2019.

482 Cook, K. H. and Vizio, E. K.: Hydrodynamics of regional and seasonal variations in Congo Basin precipitation, *Clim. Dyn.*,
483 <https://doi.org/10.1007/s00382-021-06066-3>, 2021.

484 Davies, H. C.: A lateral boundary formulation for multi-level prediction models, *Q. J. R. Meteorol. Soc.*, 102, 405–418,
485 <https://doi.org/10.1002/qj.49710243210>, 1976.

486 Davies, H. C.: Limitations of Some Common Lateral Boundary Schemes used in Regional NWP Models, *Mon. Weather Rev.*,
487 111, 1002–1012, [https://doi.org/10.1175/1520-0493\(1983\)111<1002:LOSCLB>2.0.CO;2](https://doi.org/10.1175/1520-0493(1983)111<1002:LOSCLB>2.0.CO;2), 1983.

488 Dunning, C. M., Black, E., and Allan, R. P.: Later Wet Seasons with More Intense Rainfall over Africa under Future Climate
489 Change, *J. Clim.*, 31, 9719–9738, <https://doi.org/10.1175/JCLI-D-18-0102.1>, 2018.

490 Funk, C., Peterson, P., Landsfeld, M., Pedreros, D., Verdin, J., Shukla, S., Husak, G., Rowland, J., Harrison, L., Hoell, A., and
491 Michaelsen, J.: The climate hazards infrared precipitation with stations—a new environmental record for monitoring
492 extremes, *Sci. Data*, 2, 150066, <https://doi.org/10.1038/sdata.2015.66>, 2015.

493 Günther, D., Hanzer, F., Warscher, M., Essery, R., and Strasser, U.: Including Parameter Uncertainty in an Intercomparison of
494 Physically-Based Snow Models, *Front. Earth Sci.*, 8, 2020.

495 Harris, I., Osborn, T. J., Jones, P., and Lister, D.: Version 4 of the CRU TS monthly high-resolution gridded multivariate climate
496 dataset, *Sci. Data*, 7, 109, <https://doi.org/10.1038/s41597-020-0453-3>, 2020.

497 Hersbach, H., Bell, B., Berrisford, P., Hirahara, S., Horányi, A., Muñoz-Sabater, J., Nicolas, J., Peubey, C., Radu, R., Schepers,
498 D., Simmons, A., Soci, C., Abdalla, S., Abellan, X., Balsamo, G., Bechtold, P., Biavati, G., Bidlot, J., Bonavita, M.,
499 Chiara, G. D., Dahlgren, P., Dee, D., Diamantakis, M., Dragani, R., Flemming, J., Forbes, R., Fuentes, M., Geer, A.,
500 Haimberger, L., Healy, S., Hogan, R. J., Hólm, E., Janisková, M., Keeley, S., Laloyaux, P., Lopez, P., Lupu, C.,
501 Radnoti, G., Rosnay, P. de, Rozum, I., Vamborg, F., Villaume, S., and Thépaut, J.-N.: The ERA5 global reanalysis, *Q.
502 J. R. Meteorol. Soc.*, 146, 1999–2049, <https://doi.org/10.1002/qj.3803>, 2020.

503 Howard, E. and Washington, R.: Characterizing the Synoptic Expression of the Angola Low, *J. Clim.*, 31, 7147–7165,
504 <https://doi.org/10.1175/JCLI-D-18-0017.1>, 2018.

505 Howard, E. and Washington, R.: Tracing future spring and summer drying in southern Africa to tropical lows and the Congo Air
506 Boundary, *J. Clim.*, <https://doi.org/10.1175/JCLI-D-19-0755.1>, 2019.

507 Howard, E., Washington, R., and Hodges, K. I.: Tropical Lows in Southern Africa: Tracks, Rainfall Contributions, and the Role
508 of ENSO, *J. Geophys. Res. Atmospheres*, 124, 11009–11032, <https://doi.org/10.1029/2019JD030803>, 2019.

509 Howland, M. F., Dunbar, O. R. A., and Schneider, T.: Parameter Uncertainty Quantification in an Idealized GCM With a
510 Seasonal Cycle, *J. Adv. Model. Earth Syst.*, 14, e2021MS002735, <https://doi.org/10.1029/2021MS002735>, 2022.

511 Karypidou, M. C., Katragkou, E., and Sobolowski, S. P.: Precipitation over southern Africa: is there consensus among global
512 climate models (GCMs), regional climate models (RCMs) and observational data?, *Geosci. Model Dev.*, 15, 3387–
513 3404, <https://doi.org/10.5194/gmd-15-3387-2022>, 2022.

514 Kim, Y., Rocheta, E., Evans, J. P., and Sharma, A.: Impact of bias correction of regional climate model boundary conditions on
515 the simulation of precipitation extremes, *Clim. Dyn.*, 55, 3507–3526, <https://doi.org/10.1007/s00382-020-05462-5>,
516 2020.

517 Lazenby, M. J., Todd, M. C., Chadwick, R., and Wang, Y.: Future Precipitation Projections over Central and Southern Africa and
518 the Adjacent Indian Ocean: What Causes the Changes and the Uncertainty?, *J. Clim.*, 31, 4807–4826,
519 <https://doi.org/10.1175/JCLI-D-17-0311.1>, 2018.

520 Le Coz, C. and van de Giesen, N.: Comparison of Rainfall Products over Sub-Saharan Africa, *J. Hydrometeorol.*, 21, 553–596,
521 <https://doi.org/10.1175/JHM-D-18-0256.1>, 2020.

522 Moalafhi, D. B., Evans, J. P., and Sharma, A.: Influence of reanalysis datasets on dynamically downscaling the recent past, *Clim.
523 Dyn.*, 49, 1239–1255, <https://doi.org/10.1007/s00382-016-3378-y>, 2017.

524 Munday, C. and Washington, R.: Circulation controls on southern African precipitation in coupled models: The role of the
525 Angola Low, *J. Geophys. Res. Atmospheres*, 122, 861–877, <https://doi.org/10.1002/2016JD025736>, 2017.

526 Munday, C. and Washington, R.: Systematic Climate Model Rainfall Biases over Southern Africa: Links to Moisture Circulation
527 and Topography, *J. Clim.*, 31, 7533–7548, <https://doi.org/10.1175/JCLI-D-18-0008.1>, 2018.

528 Nikulin, G., Jones, C., Giorgi, F., Asrar, G., Büchner, M., Cerezo-Mota, R., Christensen, O. B., Déqué, M., Fernandez, J.,
529 Hänsler, A., Meijgaard, E. van, Samuelsson, P., Sylla, M. B., and Sushama, L.: Precipitation Climatology in an
530 Ensemble of CORDEX-Africa Regional Climate Simulations, *J. Clim.*, 25, 6057–6078, <https://doi.org/10.1175/JCLI-D-11-00375.1>, 2012.

531 Seth, A., Rauscher, S. A., Rojas, M., Giannini, A., and Camargo, S. J.: Enhanced spring convective barrier for monsoons in a
532 warmer world?, *Clim. Change*, 104, 403–414, <https://doi.org/10.1007/s10584-010-9973-8>, 2011.

533 Van Vooren, S., Van Schaeybroeck, B., Nyssen, J., Van Ginderachter, M., and Termonia, P.: Evaluation of CORDEX rainfall in
534 northwest Ethiopia: Sensitivity to the model representation of the orography, *Int. J. Climatol.*, 39, 2569–2586,
535 <https://doi.org/10.1002/joc.5971>, 2019.

536
537

538

539

540

541

542

543

544

545

546

547

548

549

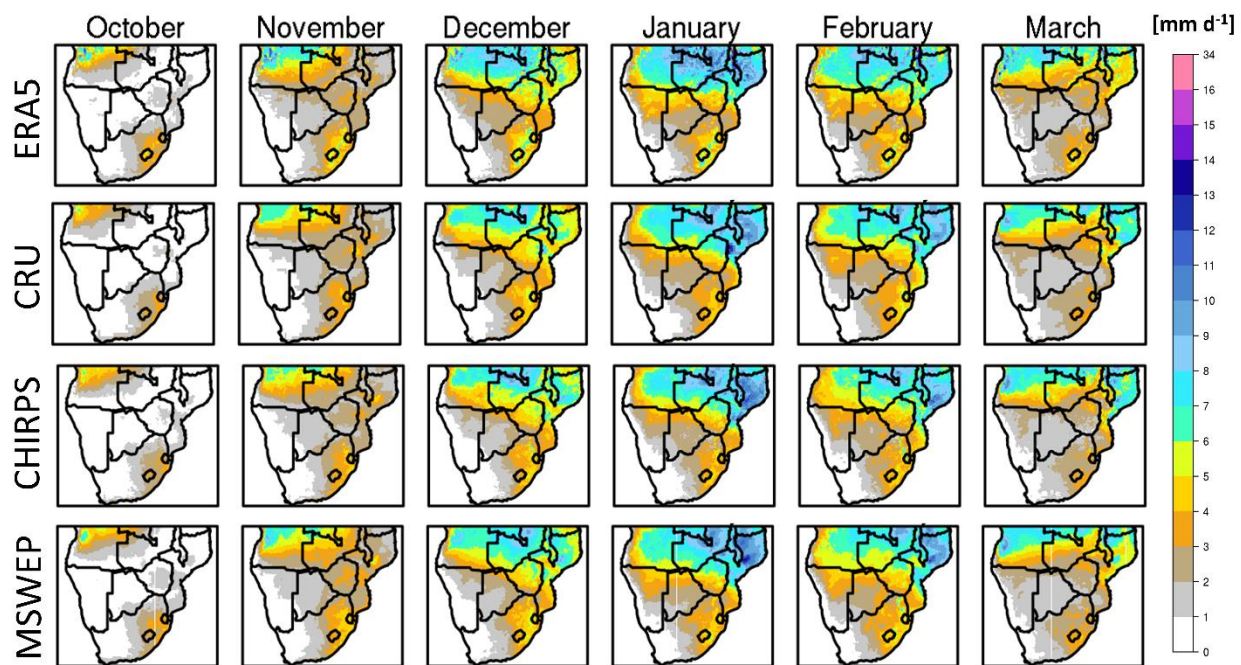
550

551

552

553

554



555

556 **Figure 1.** Monthly mean precipitation climatology for the period 1985-2005.



557

558 **Figure 2.** Study region and subregions over southern Africa.

559

560

561

562

563

564

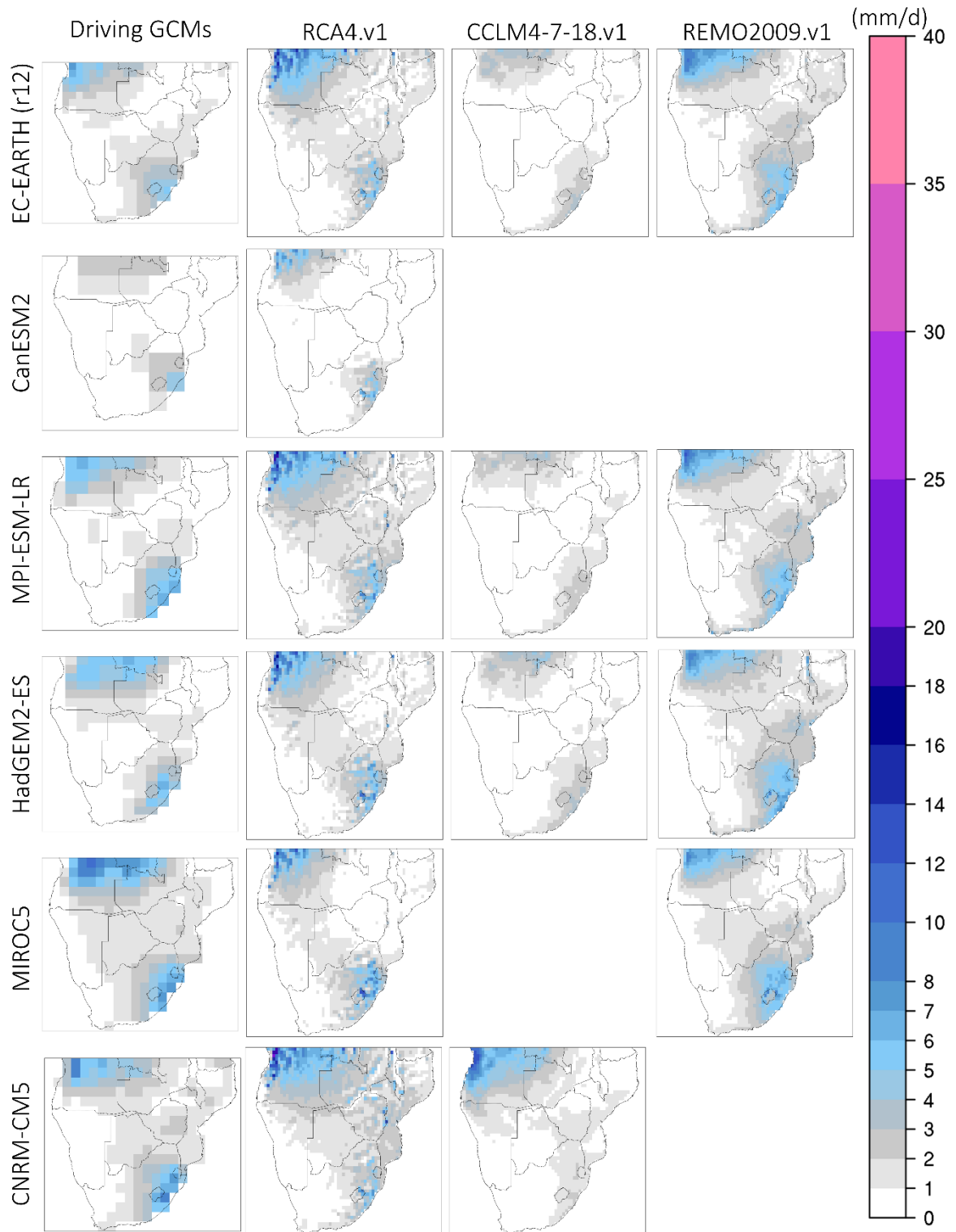
565

566

567

568

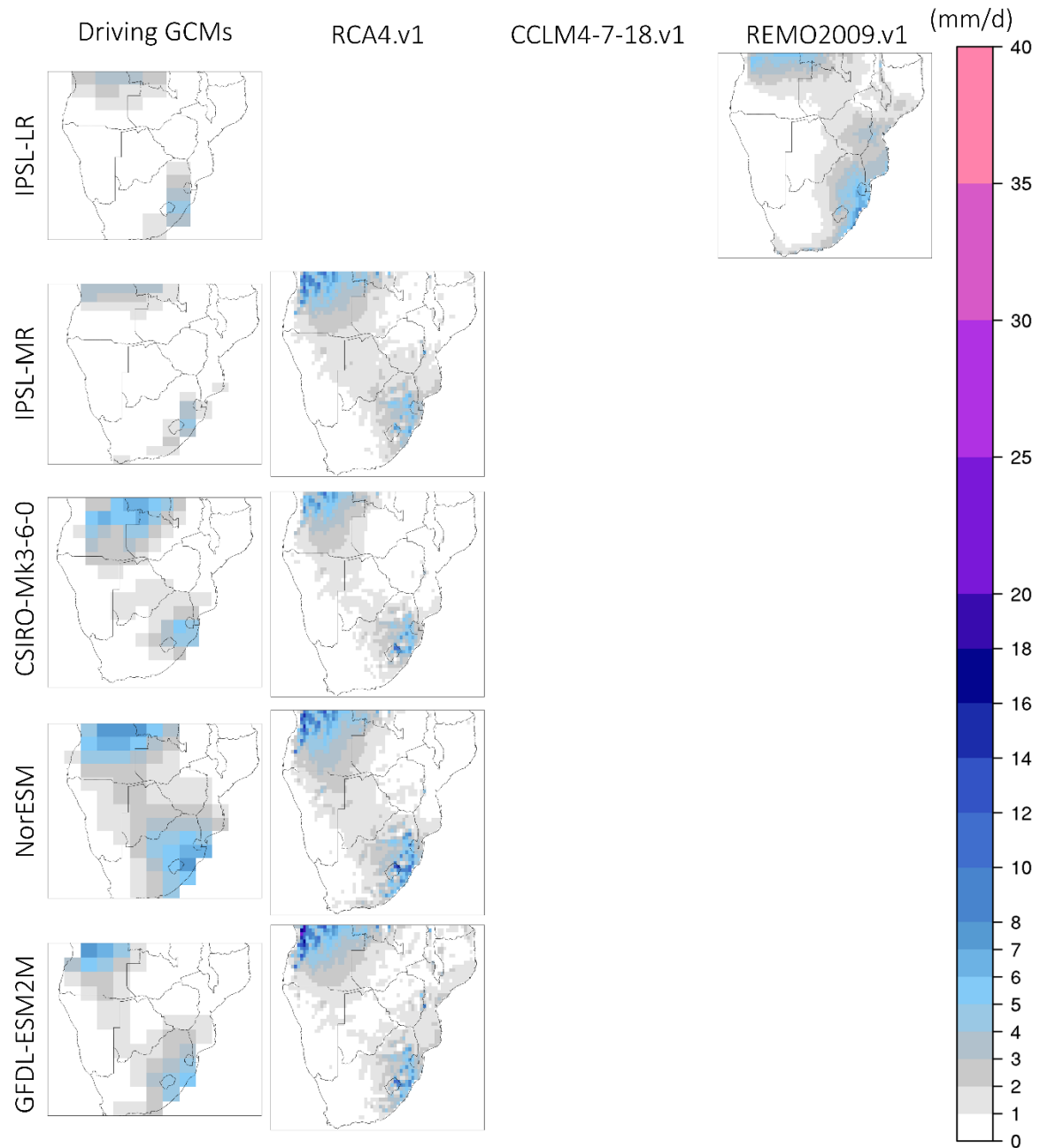
569



570

571 **Figure 3.** Monthly precipitation climatologies (mm/d) during October for the period 1985-2005. First column (from
 572 the left) displays precipitation from the driving GCMs and columns 2-4 display the downscaled precipitation output
 573 from RCA4.v1, CCLM4-8-17.v1 and REMO2009.v1.

574



575

576 **Figure 3.** Continued.

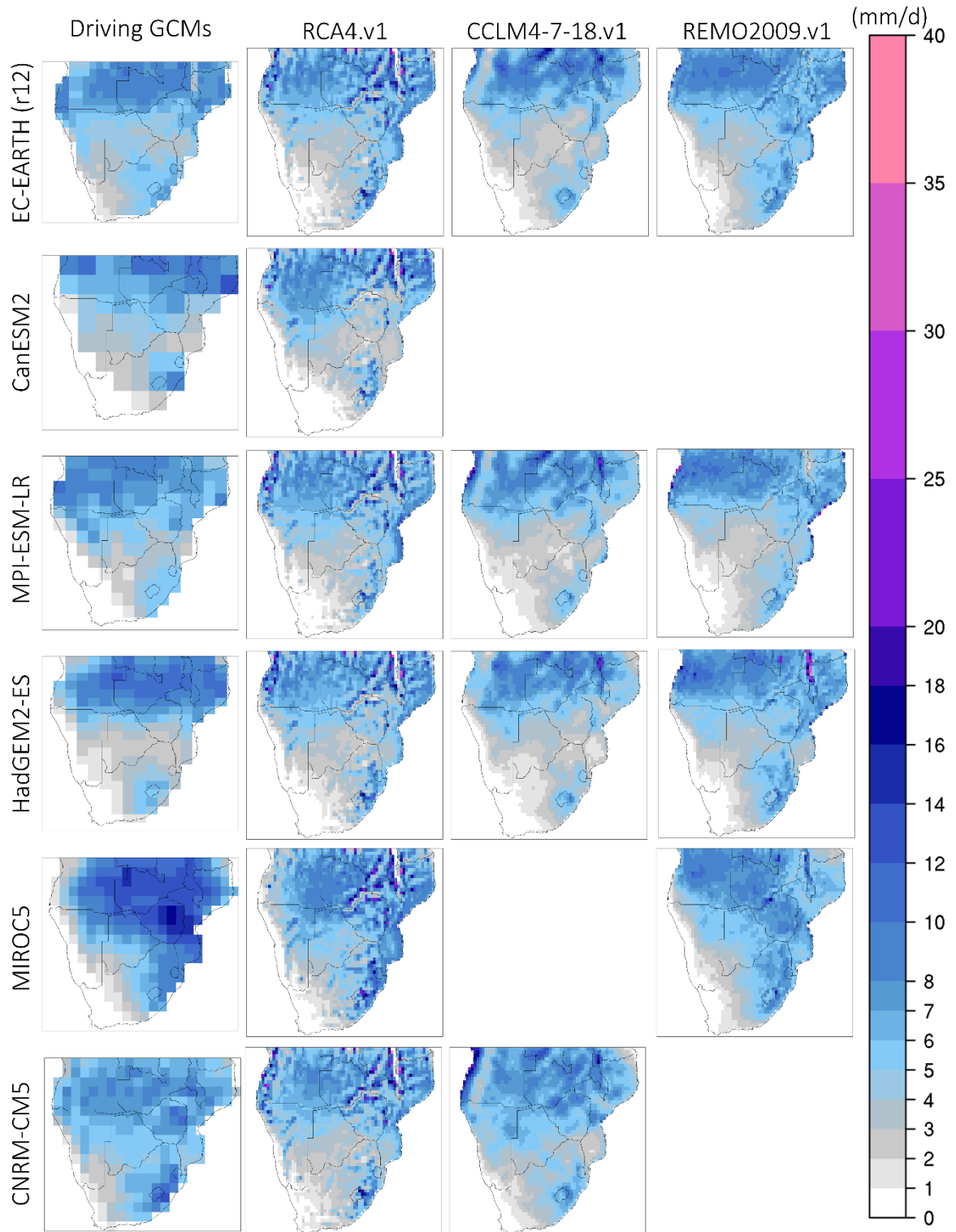
577

578

579

580

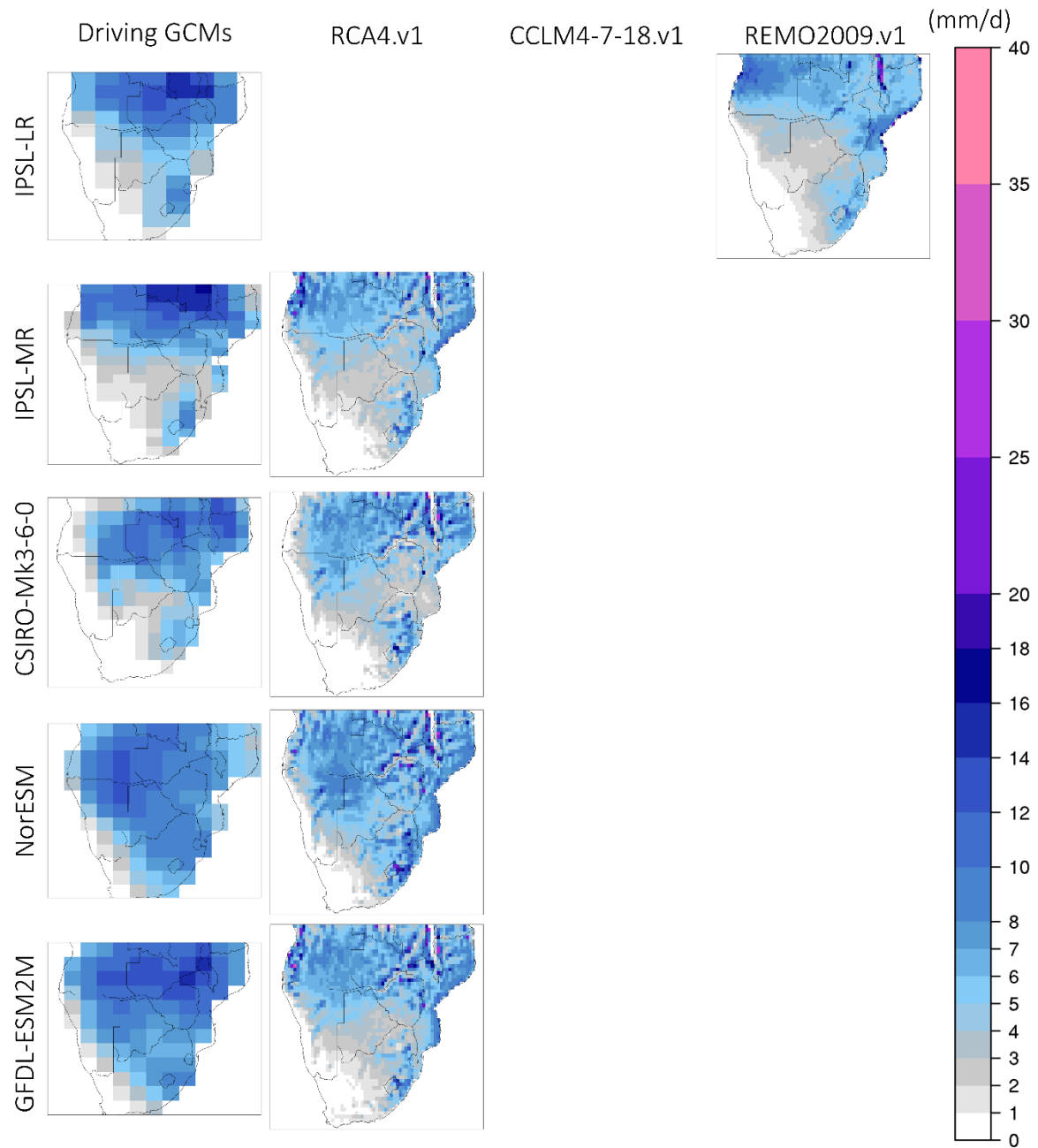
581



582

583 **Figure 4.** Monthly precipitation climatologies (mm/d) during January for the period 1985-2005. First column (from
 584 the left) displays precipitation from the driving GCMs and columns 2-4 display the downscaled precipitation output
 585 from RCA4.v1, CCLM4-8-17.v1 and REMO2009.v1.

586



587

588 **Figure 4.** Continued.

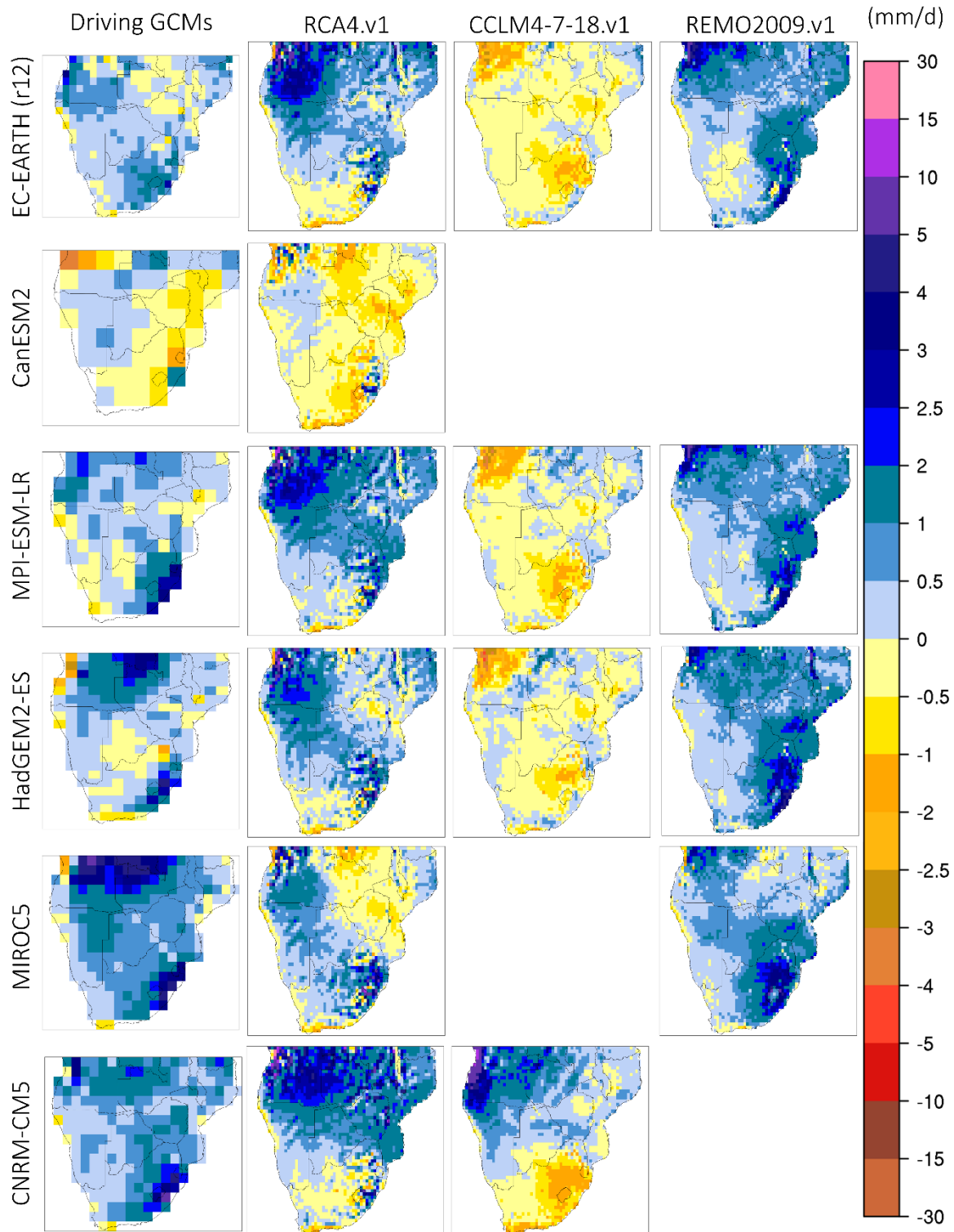
589

590

591

592

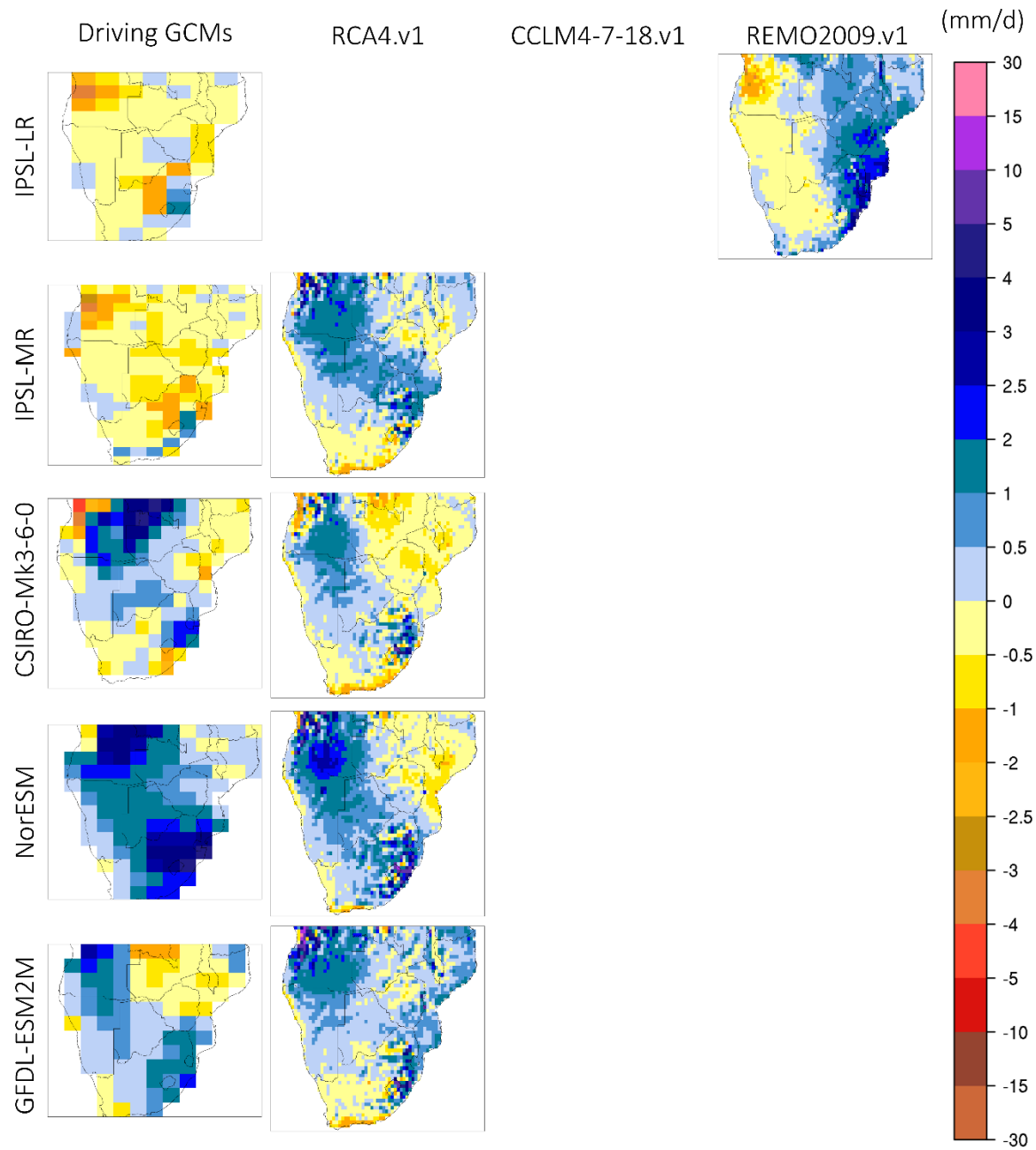
593



594

595 **Figure 5.** Monthly precipitation bias (model – CHIRPS in mm/d) during October for the period 1985-2005. First
 596 column (from the left) displays the biases in the driving GCMs and columns 2-4 display the biases in the downscaled
 597 precipitation output according to RCA4.v1, CCLM4-8-17.v1 and REMO2009.v1.

598



599

600 **Figure 5.** Continued.

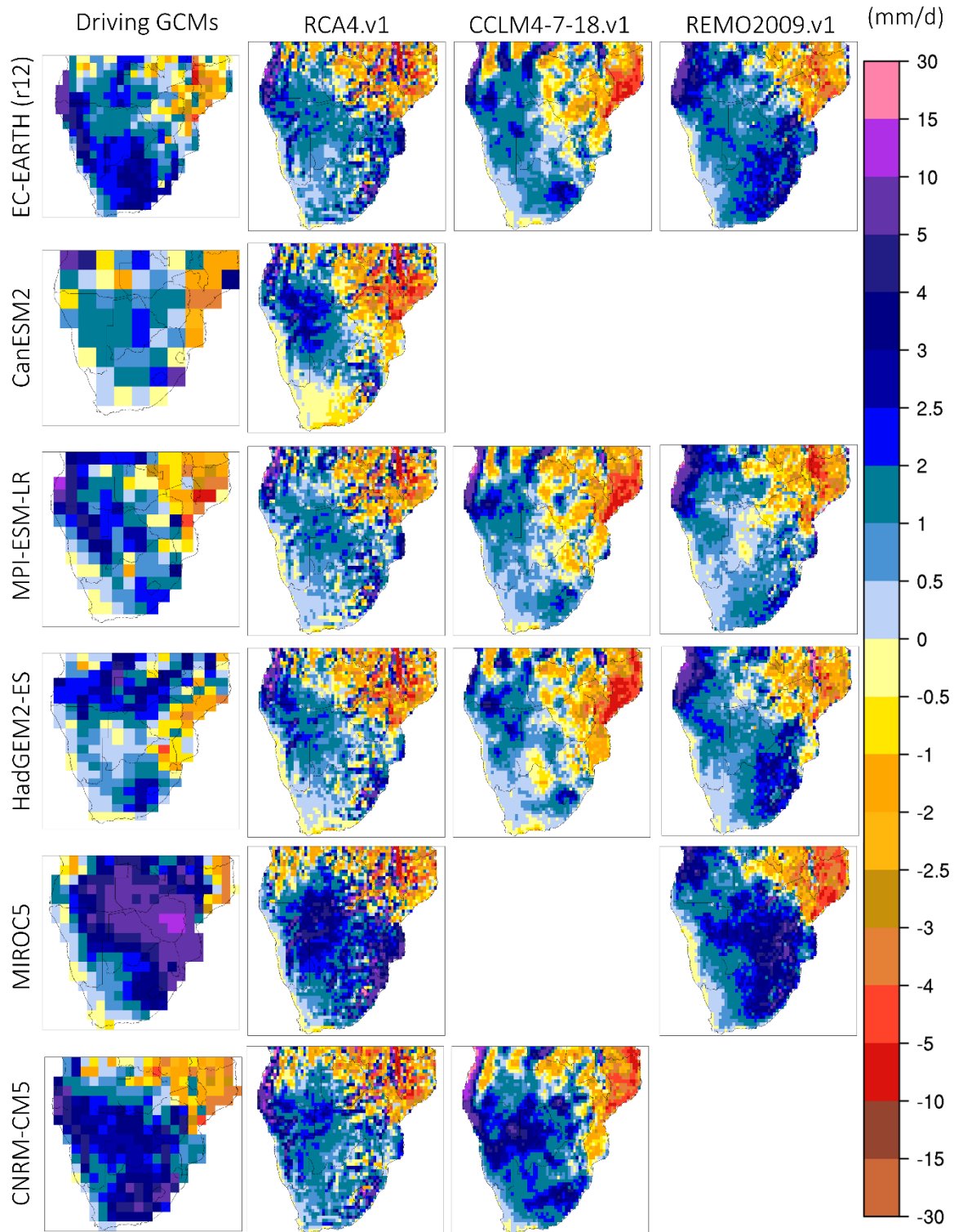
601

602

603

604

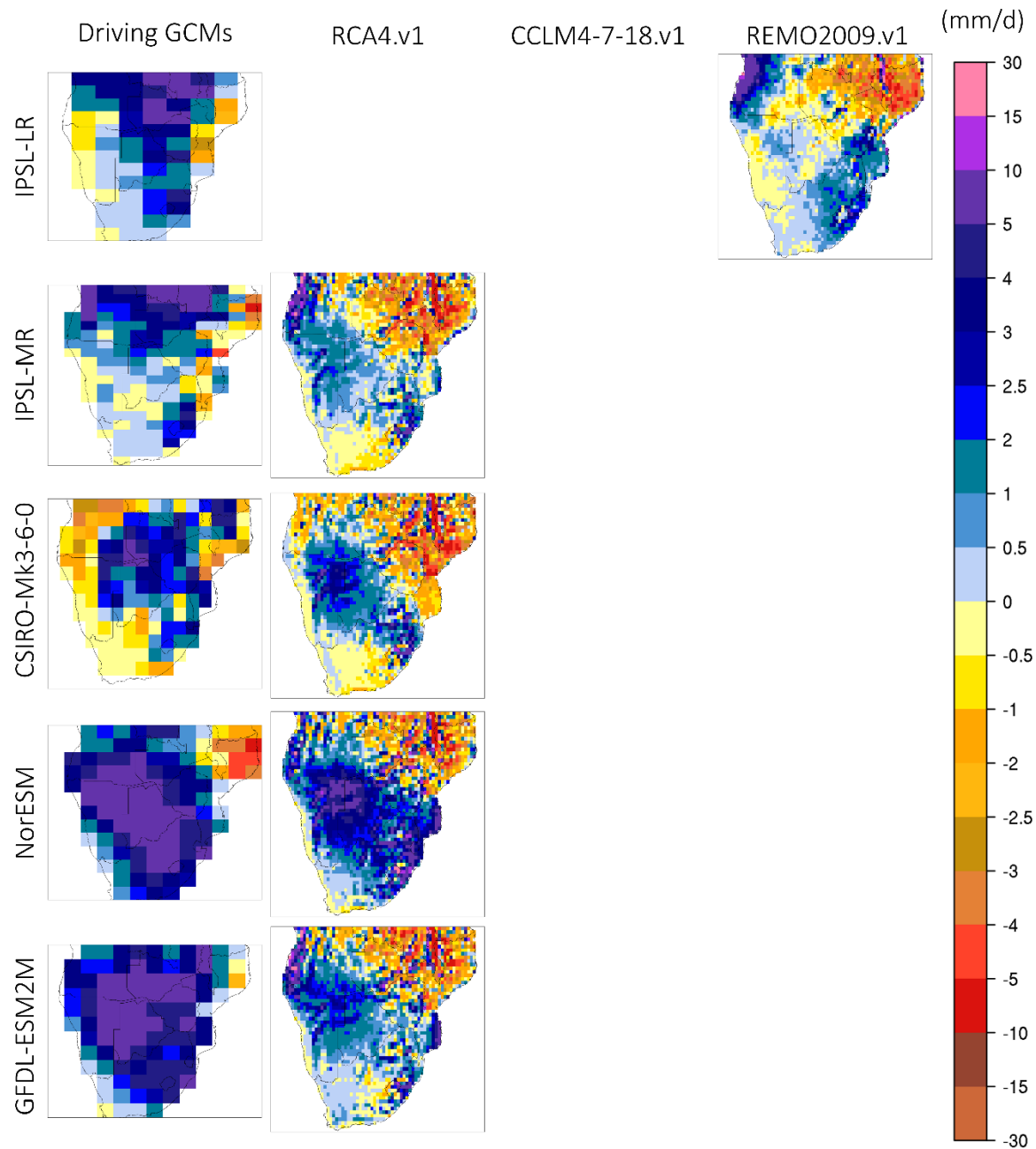
605



606

607 **Figure 6.** Monthly precipitation biases (model - CHIRPS in mm/d) during January for the period 1985-2005. First
 608 column (from the left) displays precipitation biases from the driving GCMs used and columns 2-4 display the
 609 downscaled products according to RCA4.v1, CCLM4-8-17.v1 and REMO2009.v1.

610



611

612 **Figure 6.** Continued.

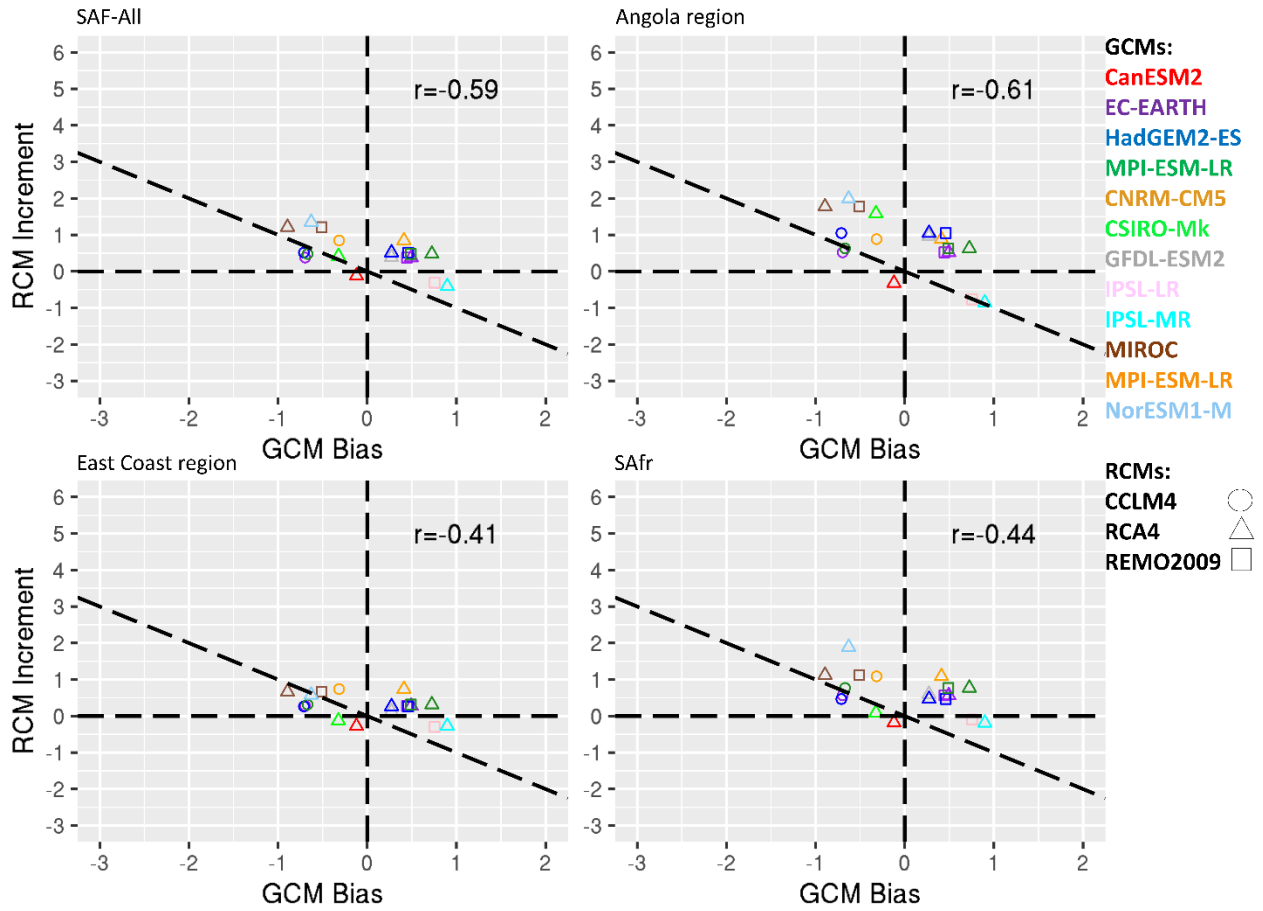
613

614

615

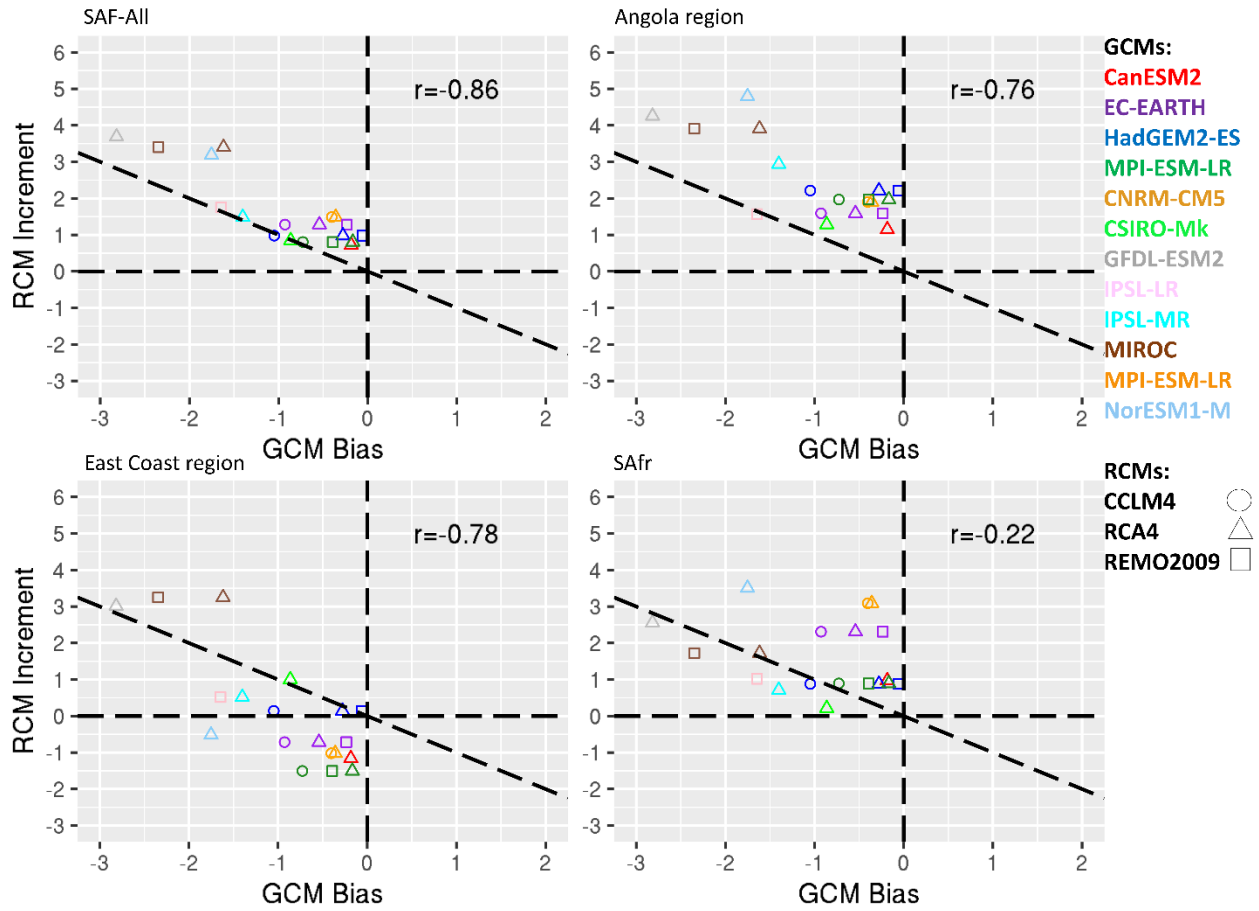
616

617



618

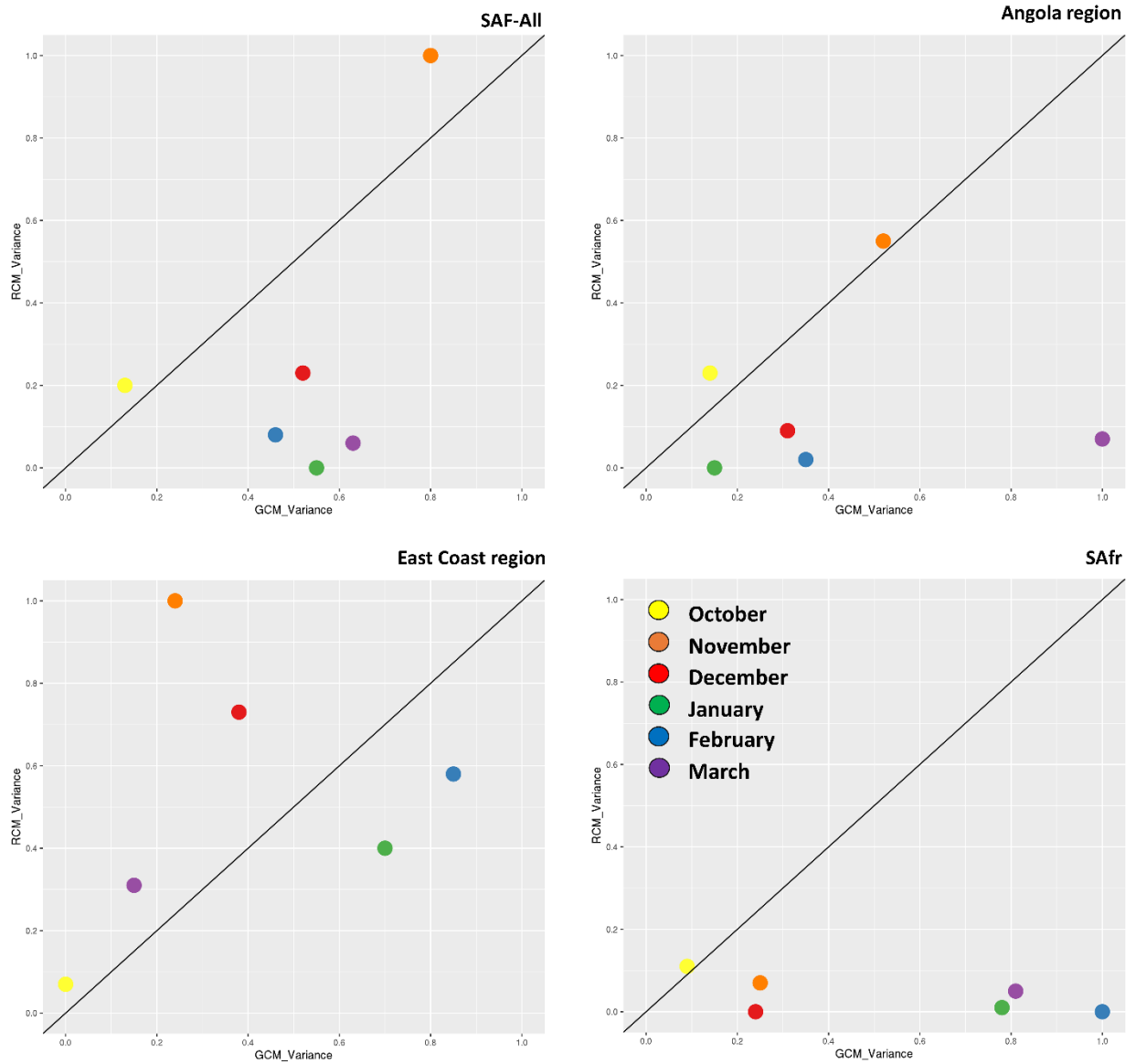
619 **Figure 7.** Scatterplots of the RCM increment (RCM-GCM) for precipitation (mm/day) as a function of the GCM bias
 620 (GCM-OBS) for October. Colors indicate the driving GCM and shapes indicate the downscaling RCMs. The four
 621 panels indicate spatial averages over southern Africa (SAF-All region), the Angola region, the East Coast region and
 622 the SAfr region.



623

624 **Figure 8.** Scatterplots of the RCM increment (RCM-GCM) for precipitation (mm/day) as a function of the GCM bias
 625 (GCM-OBS) for January. Colors indicate the driving GCM and shapes indicate the downscaling RCMs. The four
 626 panels indicate spatial averages over southern Africa (SAF-All region), the Angola region , the East Coast region and
 627 the SAfr region.

628



629

630 **Figure 9.** Analysis of variance for monthly precipitation during 1985-2005 for southern Africa (SAF-All region) and
 631 the 3 sub-regions examined, namely the Angola region, East Coast region and the SAfr region.. The x and y-axis
 632 display standardized precipitation variances.

633

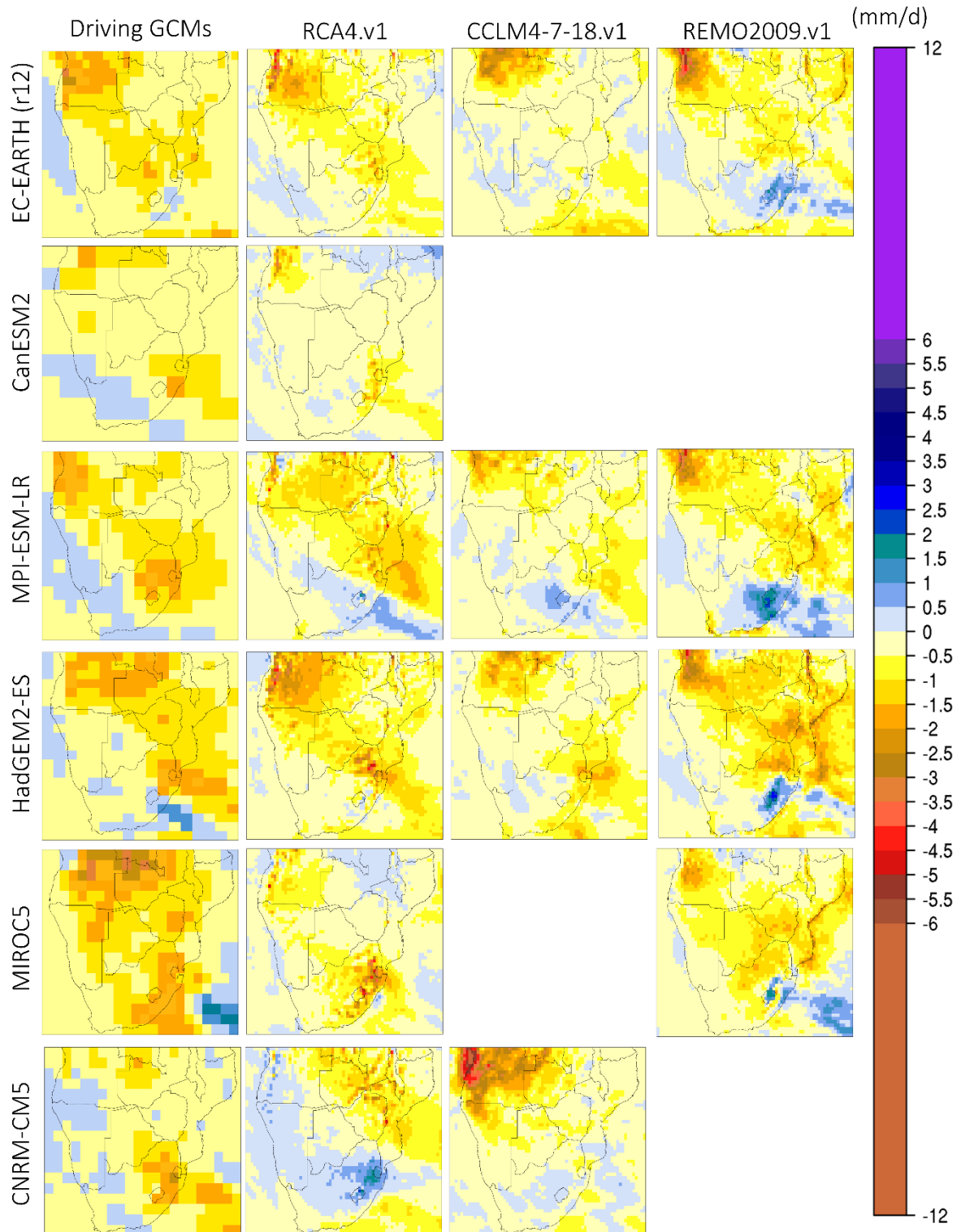
634

635

636

637

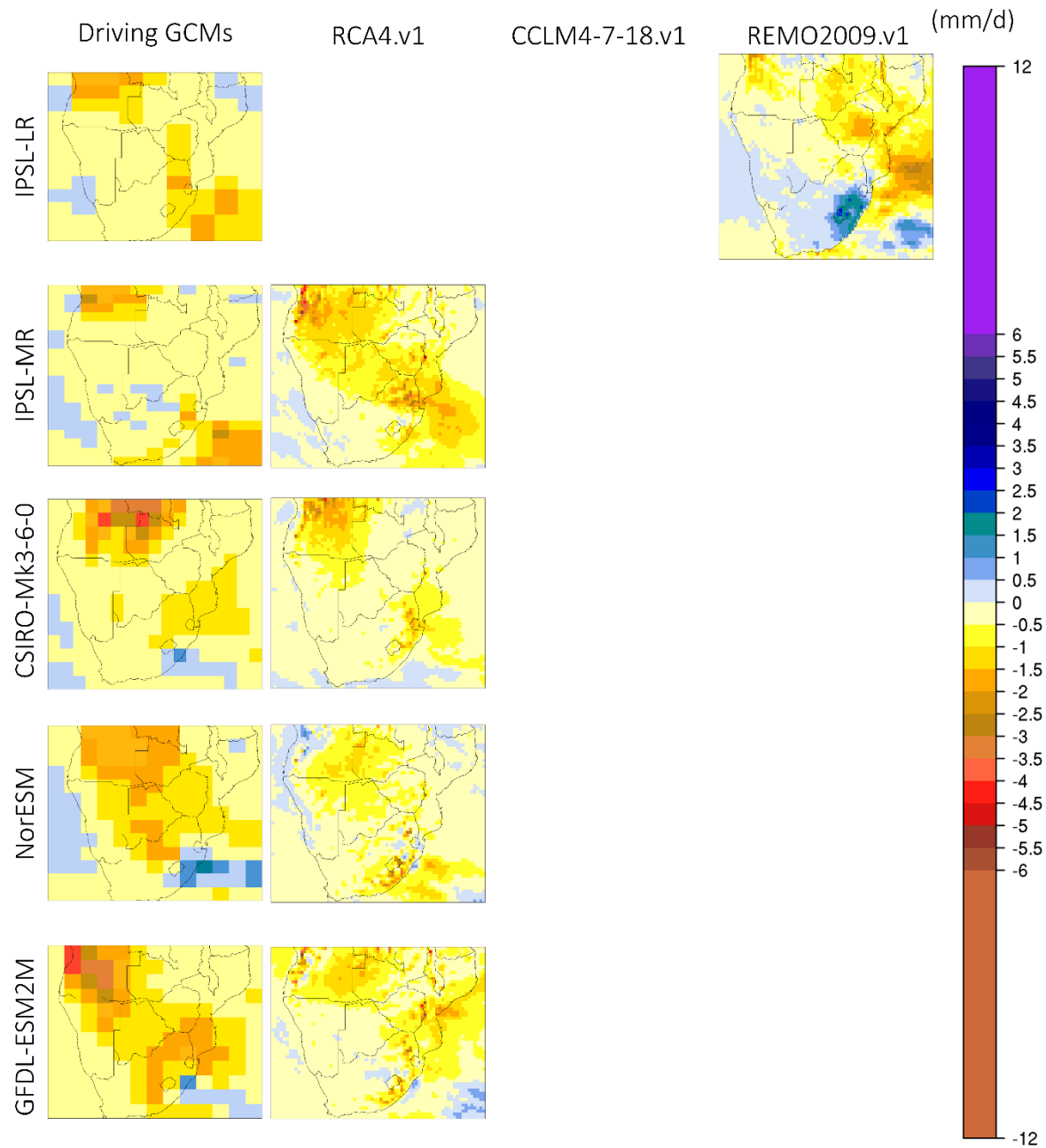
638



639

640 **Figure 10.** Monthly precipitation change (future – present in mm/d) during October for the period 2065-2095 relative
 641 to 1985-2005. First column (from the left) displays precipitation change from the driving GCMs used and columns 2-
 642 4 display the downscaled products according to RCA4.v1, CCLM4-8-17.v1 and REMO2009.v1.

643



644

645 **Figure 10.** Continued.

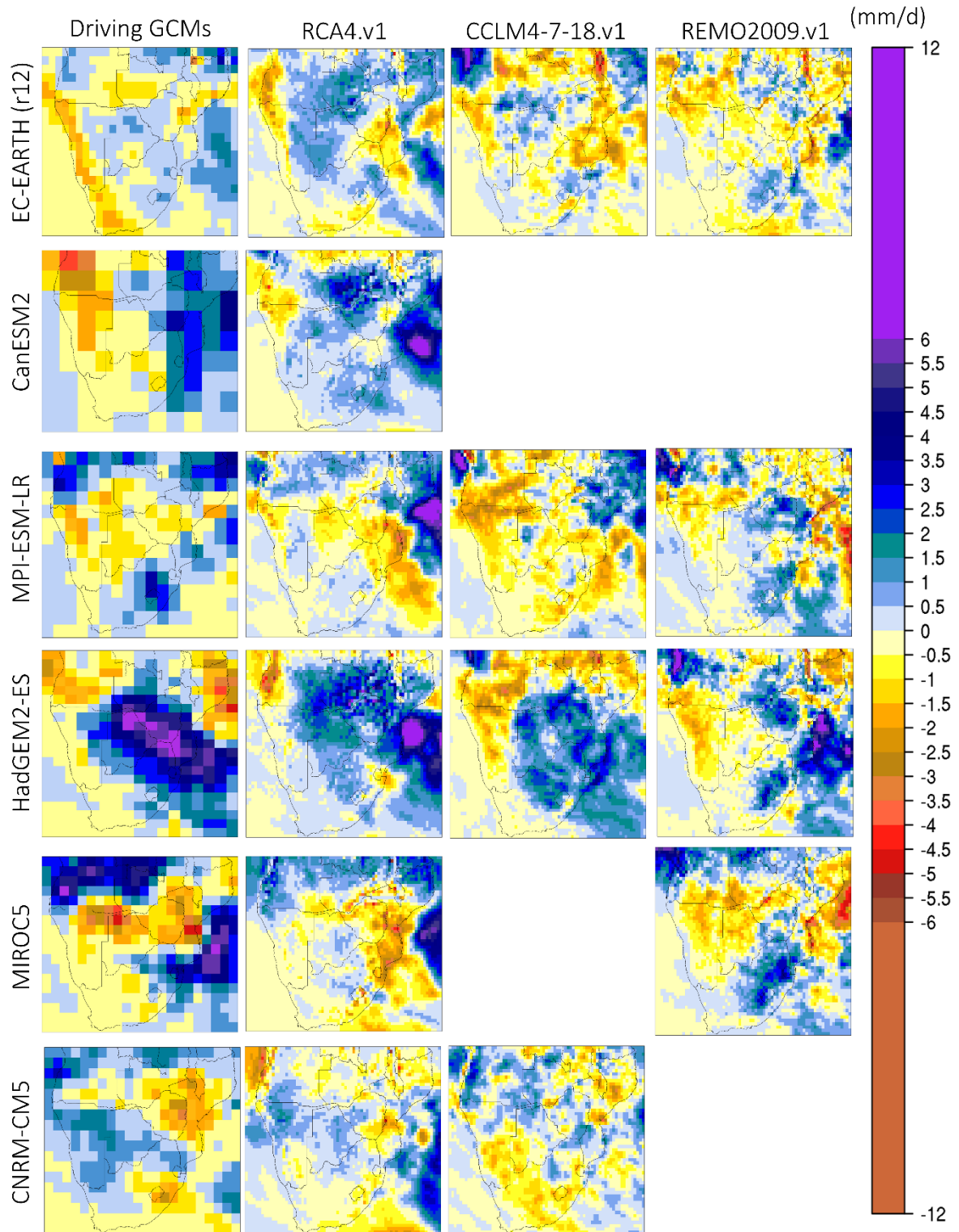
646

647

648

649

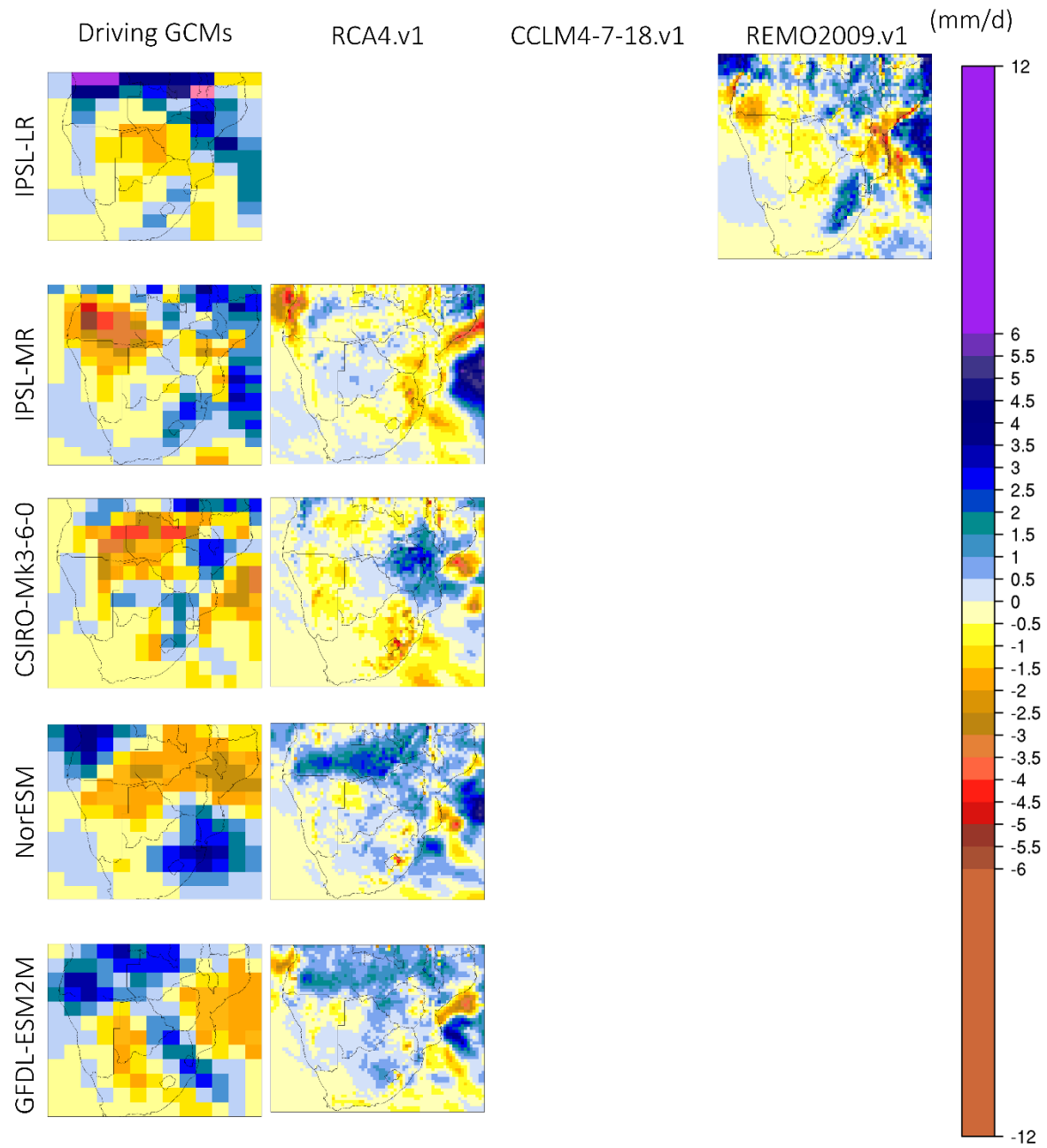
650



651

652 **Figure 11.** Monthly precipitation change (future – present in mm/d) during January for the period 2065-2095 relative
 653 to 1985-2005. First column (from the left) displays precipitation change from the driving GCMs used and columns 2-
 654 4 display the downscaled products according to RCA4.v1, CCLM4-8-17.v1 and REMO2009.v1.

655



656

657 **Figure 11.** Continued.

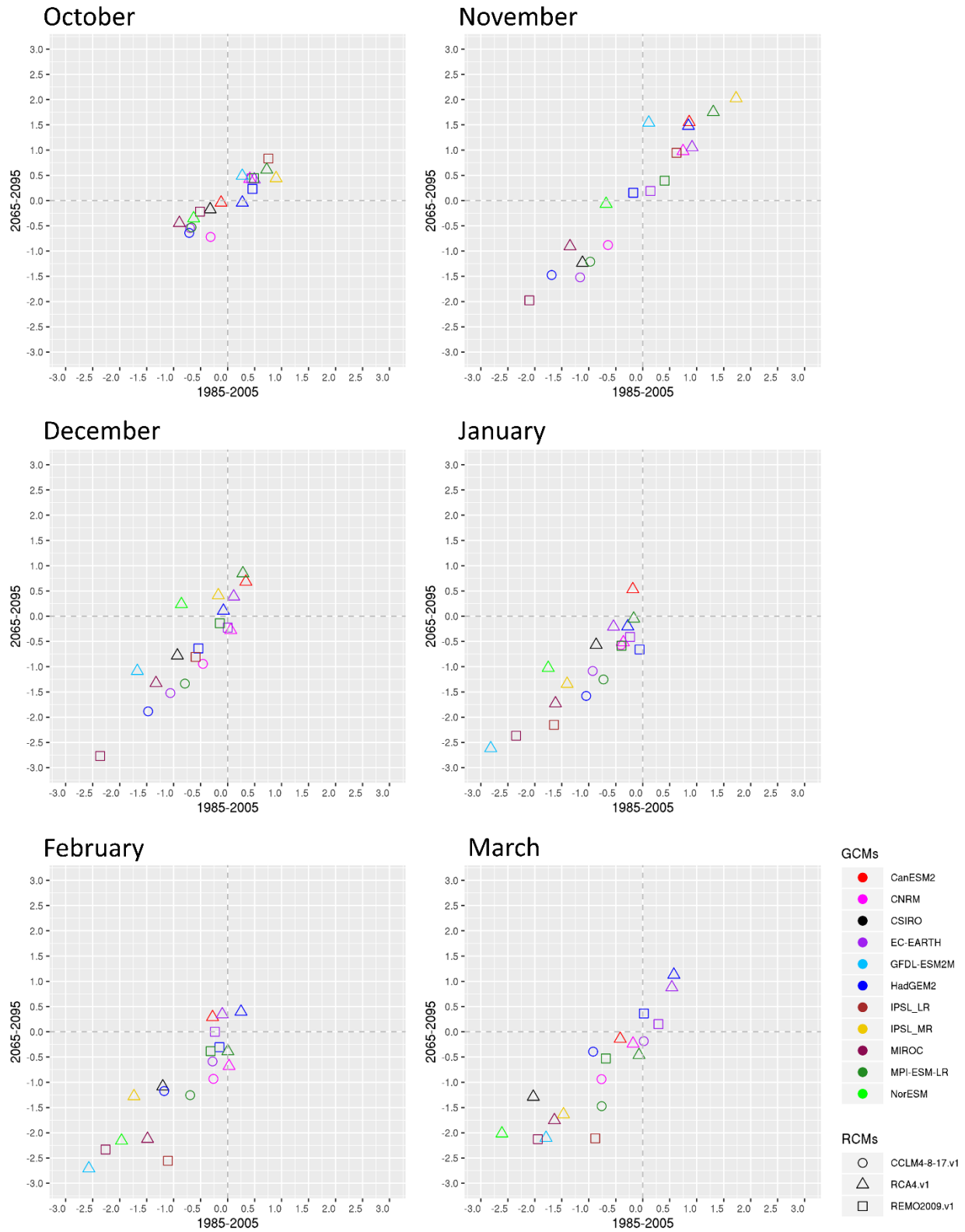
658

659

660

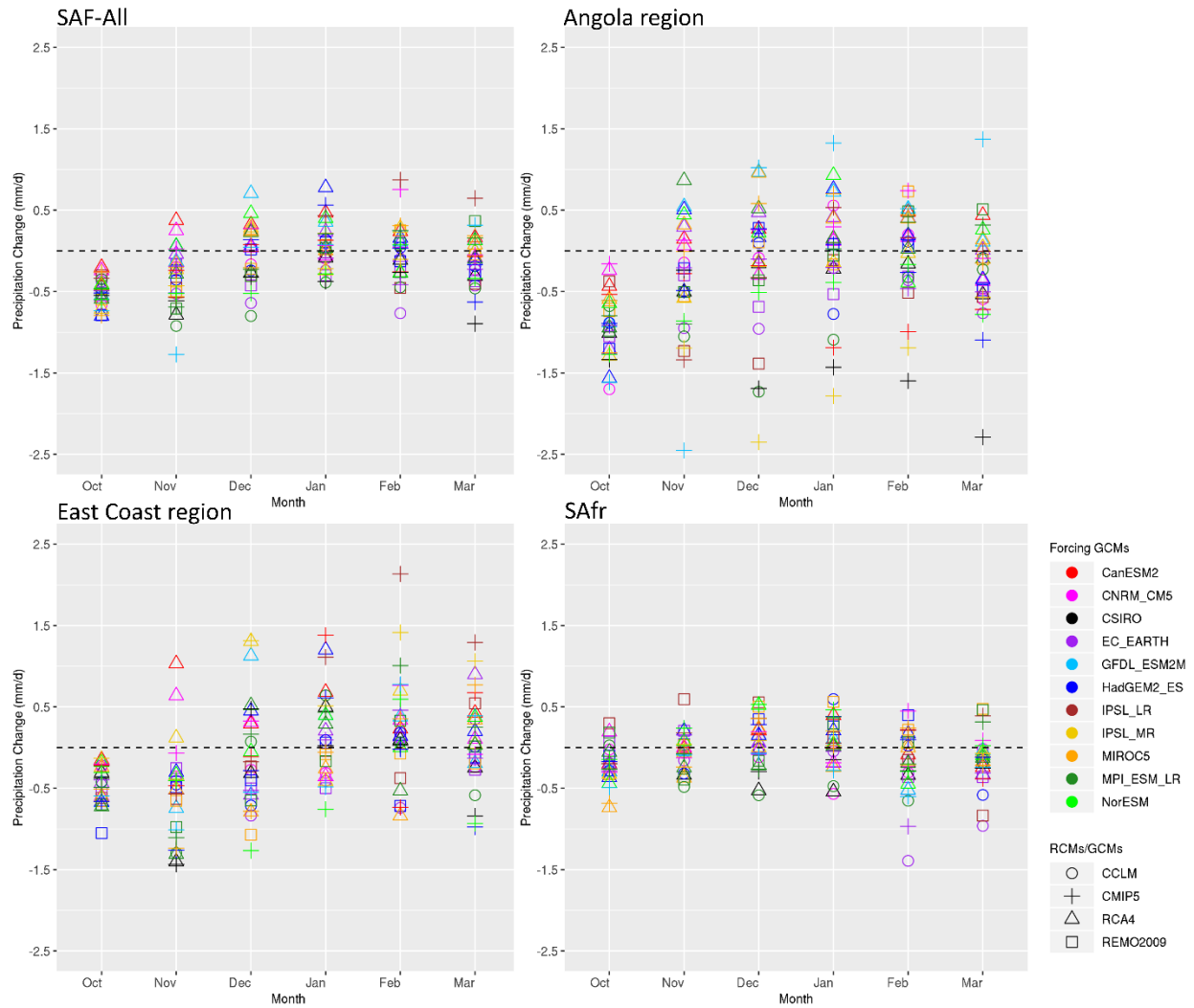
661

662



663

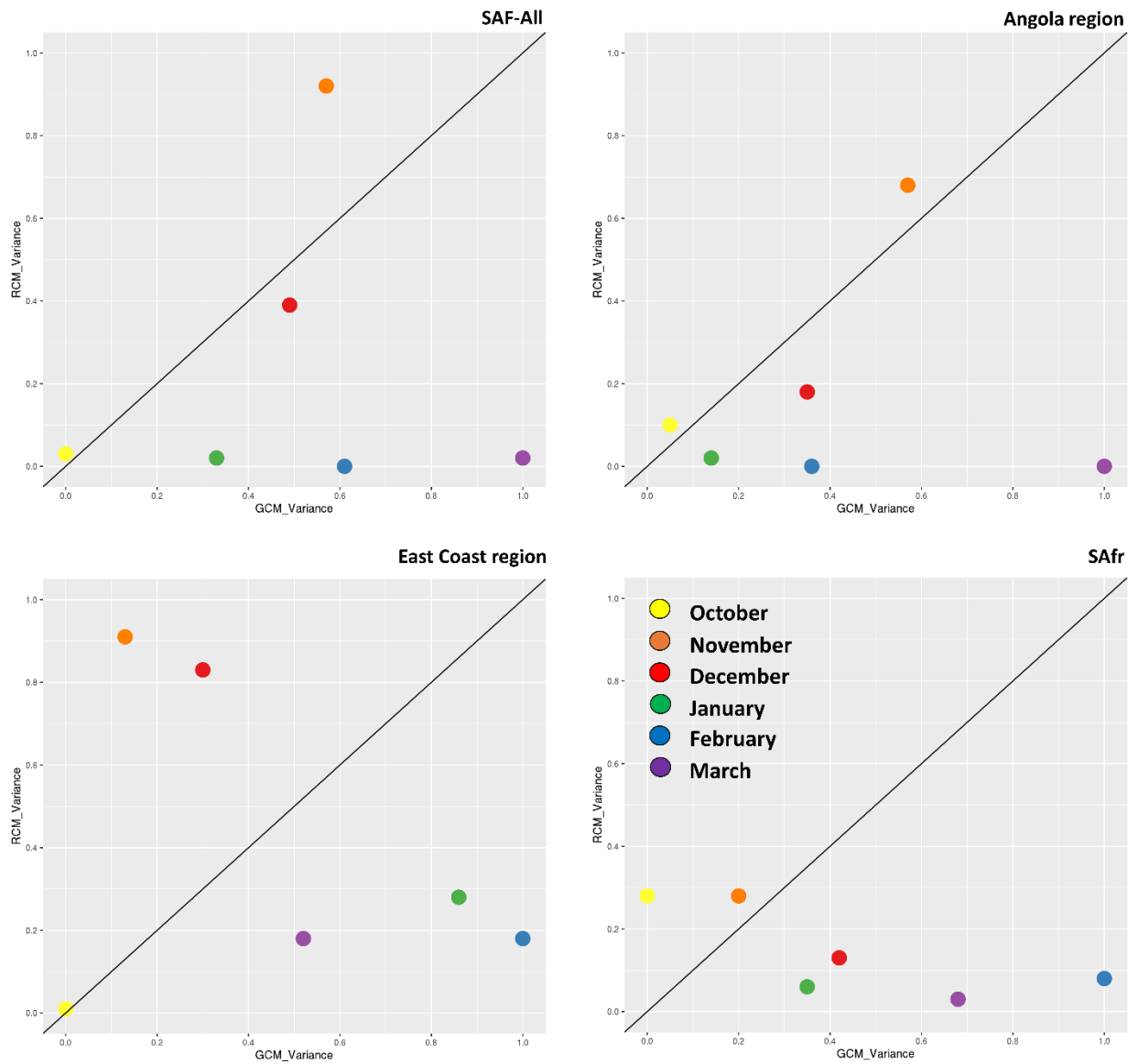
664 **Figure 12.** Monthly $RCM_{DRI} - DRI$ spatial averages over southern Africa for the historical period (1985-2005) on the
 665 x-axis and the future period (2065-2095) under RCP8.5 on the y-axis.



666

667
668

Figure 13. Spatial average of the precipitation change signal (mm/d) from RCMs and their driving GCMs relative to 1985-2005 for southern Africa and the 3 sub-regions examined.



669

670 **Figure 14.** Analysis of variance for monthly precipitation during 2065-2095 for southern Africa (SAF-All region) and
 671 the 3 sub-regions examined, namely the Angola region, East Coast region and the SAfr region.. The x and y-axis
 672 display standardized precipitation variances.

673

674